What's new?

Cancer-related inflammation helps tumors spread like wildfire, and TNF-α gets that inflammation going. In some cancers, TNF-α drives cells toward metastasis and boosts expression of CD44, a marker of cancer stem cells. What is the role of TNF-α in clear cell renal cell carcinoma (ccRCC)? These authors found that TNF-α expression correlates with CD44 expression, and both are associated with tumor stage and poor prognosis. In addition, when patients were treated with sunitinib, the ones that didn't respond well to the treatment had high CD44 expression, suggesting that TNF-α can bolster chemotherapy resistance by driving up CD44 levels.

is also reported to modulate expression of CD44, a marker of cancer stem cell, in carcinomas of the breast and ovary.[5–7] However, expression of TNF-α in RCC tissues and its association with clinicopathological parameters including prognosis remain elusive.[8] In addition, little or no information is available for the association between TNF-α and CD44 in ccRCCs.

Sunitinib, an inhibitor of multi-targeted tyrosine kinases such as receptors for vascular endothelial growth factor (VEGF) and platelet-derived growth factor (PDGF)[9], is now used as a molecular target therapy for the patients with advanced ccRCC because of its superiority over the cytokine-mediated approaches.[10] However, most patients treated with sunitinib acquire resistance to the treatment commonly in 6 - 11 months after the treatment.[11] Although investigation of the ccRCC tissues removed from sunitinib-treated patients is important to study the mechanism of the resistance, there is only one report that described a decrease in angiogenesis in ccRCCs treated with sunitinib.[12]

In the present study, we have demonstrated that the expression of TNF-α and CD44 is predominantly observed in high-grade ccRCCs, showing positive correlation each other and inverse correlation with progression-free and overall survivals. TNF-α induced EMT in two ccRCC cell lines together with increased expression of CD44 and TNF-α. In addition, TNF-α and CD44 were highly expressed by residual carcinoma cells in metastatic ccRCC tissues removed from the patients with sunitinib treatment. These data suggest that the TNF-α/CD44 axis may be associated with progression of ccRCCs and that CD44 induced by TNF-α may be involved in the resistance to the sunitinib treatment in ccRCCs.

Material and Methods

Patients

Renal specimens were obtained by total or partial nephrectomy from 120 patients, who were clinically and pathologically diagnosed as having ccRCC from 1991 to 2003 in Keio University Hospital. The International Union Against Cancer tumor-node-metastases (TNM) system was used for tumor staging,[13] and nuclear grading was performed according to the nuclear grading method reported by Fuhrman *et al.*[14] Their clinicopathological parameters at the time of nephrectomy were summarized in Supporting Information Table 1S. During the follow-up periods, 45 patients developed metastatic disease, and 23 patients died of disease. Metastases were removed without treatment in 11 patients. Twenty-five patients were treated with sunitinib, and 10 metastases were removed after the treatment. Other nine patients were treated with interferon-α or interleukin-2. Sunitinib was administered according to the protocol described previously,[10] and the effect was assessed according to the Response Evaluation Criteria in Solid Tumors.[15] Time to treatment failure was defined as the period between treatment initiation and tumor progression, drug cessation or death. Overall survival for evaluation of sunitinib was defined as the period between sunitinib initiation and the date of last-follow up or death. Sunitinib treatment was discontinued in 15 patients (non-responders) because of progressive disease (10 cases) and severe adverse effect (5 cases), and the treatment has been continued in other 10 patients (responders). Among the 25 patients treated with sunitinib, 11 patients died of the disease. This study was performed after approval by the Institutional Review Board of the Keio University Hospital and informed consent for experimental use of the samples was obtained from the patients according to the hospital's ethical guidelines.

Immunohistochemistry

Paraffin sections of cancer tissues were obtained from the 120 primary ccRCC patients, 11 untreated metastatic ccRCC patients (3 bone, 3 lung, 2 brain, 2 pancreas or 1 adrenal metastases) and 10 sunitinib-treated metastatic ccRCC patients (6 bone, 2 skin 1 lung or 1 small intestine metastases). Sections were immunostained with anti-TNF-α mouse monoclonal antibody (2 μg/ml; clone CH8810, Abnova Corp., Taipei, Taiwan), anti-CD44 mouse monoclonal antibody (2 μg/ml; clone DF1485, Santa Cruz Biotechonologies, Santa Cruz, CA), anti-E-cadherin mouse monoclonal antibody (1.25 μg/ml; clone 36/E-cadherin, BD Biosciences, San Jose, CA), or anti-N-cadherin mouse monoclonal antibody (4.0 μg/ml; clone 6G11, DAKO, Glostrup, Denmark) as described previously.[16] For negative controls, tissues were incubated with non-immune mouse IgG (Sigma-Aldrich, St. Louis, MO) at the same concentration used for each antibody.

To evaluate TNF-α immunostaining, carcinoma cells with cytoplasmic staining were counted at least in 10 representative fields (400× magnification), and the mean percentage of TNF-α-positive cancer cells in the field was calculated.

For CD44, E-cadherin and N-cadherin staining, the mean percentage of positive cells was calculated by counting carcinoma cells with cell surface staining. Because CD44 was expressed by macrophages infiltrating within ccRCC tissues, the number of CD44-positive macrophages was determined in 10 representative areas (400× magnification), and the average number was calculated (cells/0.24 mm^2). In representative sections, immunostaining of CD68 (1.0 μg/ml; clone pgm1, DAKO) was also performed to confirm that CD44-positive tumor infiltrating cells were marcophages (data not shown). The cases in which the TNF-α-, CD44-, E-cadherin- or N-cadherin-positive carcinoma cell ratio was equal to or more than the mean were defined as TNF-α, CD44-high, E-cadherin-high or N-cadherin high cases and those less than mean were defined as low cases.

Cell Cultures and Assays for Migration and Invasion

Human ccRCC cell lines, 786-O cells with inactive mutation of von-Hippel Lindau (VHL) gene and ACHN cells with wild type VHL gene, were obtained from American Type Culture Collection (Manassas, VA), and cultured as described preciously.[17] For hypoxic treatment, 786-O cells were cultured in an anaerobic environmental chamber maintained with 1% O_2, 94% N_2 and 5% CO_2 for 8 h. Human recombinant TNF-α (R&D systems, Minneapolis, MN) was added to serum-free culture medium. Migration and invasion assays were performed using transwell cell culture inserts 8 μm pore-size non-coated polyethylene terephthalate (PET) membrane (Coster, Corning Inc., Corning, NY) and inserts with 8 μm pore-size PET membrane coated with a uniform layer of BD Matrigel™ Basement Membrane Matrix (BD Biosciences, San Jose, CA) as described previously.[16]

Quantitative Real-Time PCR

Total RNA was isolated from ccRCC cell lines and reverse-transcribed to complementary DNA (cDNA), and it was amplified in a TaqMan quantitative real-time PCR assay using ABI Prism 7000 Sequence Detection System (Life technologies Corporation, Carlsbad, CA) as described previously.[16] The primers and TaqMan Probe sets (TaqMan Gene Expression Assays Inventories) for TNF-α (Hs00174128_m1), CD44 (Hs01075861_m1), MMP9 (Hs00234579_m1), vimentin (Hs00185584_m1), E-cadherin (Hs010234579_m1), N-cadherin (Hs00983056_m1), fibronectin (Hs01547673_m1), and human β-actin (4310881E) were purchased from Life technologies (sequences not disclosed). The relative quantification values of each gene were normalized against that of β-actin, an endogenous control.

Immunoblotting

Proteins in the samples were resolved by sodium dodecyl sulfate-polyacrylamide gel electrophoresis (7.5% total acrylamide) under reduction, followed by transfer onto polyvinylidene difluoride membranes. Immunoblotting was performed by incubation of the membrane with anti-E-cadherin mouse monoclonal antibody (1.25 μg/ml; clone 36/E-cadherin, BD Bioscience), anti-N-cadherin mouse monoclonal antibody (1.0 μg/ml; clone 6G11, DAKO), anti-vimentin mouse monoclonal antibody (1.0 μg/ml; clone V9, DAKO), anti-fibronectin mouse monoclonal antibody (1.0 μg/ml; clone EP5, Santa Cruz Biotechnologies), anti-CD44 mouse monoclonal antibody (0.5 μg/ml, SantaCruz Biotechnologies) or anti-β-actin mouse monoclonal antibody (1.0 μg/ml, Sigma-Aldrich). The immunoreactive protein bands were detected with enhanced chemiluminescence immunoblotting Western blotting reagents (Amersham, Piscataway, NJ), and densitometrically analyzed with Image J software.

Statistical Analysis

Mann-Whitney's *U*-test was used to analyze the relationships between expression levels of TNF-α−, E-cadherin-, N-cadherin- or CD44-positive tumor cell ratio and clinicopathological parameters. *In vitro* results were expressed as mean ± standard deviation (SD). Student's *t*-test was used for analyses related to *in vitro* experiments. The log-rank test and Kaplan-Meier method were used for survival analyses. Univariate and multivariate analyses were done according to Cox proportional hazard analysis. The prognostic significance of TNF-α and CD44 expression was also evaluated after adjusting for a known predictor of ccRCC outcome, Mayo Clinic stage, size, grade, and necrosis (SSIGN) score.[18] *p* Values below 0.05 were considered to be significant. StatView for Windows (version 5.0; Abacus Concepts, Inc., Berkeley, CA) was used to calculate statistical differences between groups.

Results

Immunohistochemical Expression of TNF-α, CD44, E-cadherin and N-cadherin in ccRCCs

TNF-α immunostaining in cytoplasm of cancer cells was observed in 96 of 120 ccRCCs (80%). Cancer cells in low-grade (Grades 1 and 2) ccRCCs were mostly negative for TNF-α staining (Fig. 1*a*), but high-grade (Grades 3 and 4) ccRCCs showed diffuse TNF-α staining (Fig. 1*b*). Cell surface CD44 staining in cancer cells was found in 65 of 120 ccRCCs (54%). Most cancer cells in low-grade ccRCCs were negative for CD44 staining (Fig. 1*c*), but high-grade ccRCCs were positive (Fig. 1*d*). CD44-positive cancer cell ratio was significantly higher in high-grade ccRCCs (26.6 ± 29.2%) (mean ± SD) than that in low-grade ccRCCs (3.4 ± 9.5%) ($p < 0.001$). Infiltrated macrophages within tumor tissues showed positive staining of CD44. Mean number of CD44-positive marcophages within high-grade ccRCCs tissues (25.1 ± 22.5 cells/0.24 mm^2) was significantly higher than that in low-grade tumors (12.5 ± 17.6 cells/0.24 mm^2) ($p < 0.001$). SD of CD44-positive cancer cells and the number of macrophages within ccRCC tissues were relatively high compared to the mean. This may be due to that CD44 expression in cancer cells and macrophages were low in many ccRCCs, and relatively small numbers showed high CD44 expression (data not shown). Cell surface E-cadherin staining was observed in 51% of the cases (61 of 120 ccRCCs). Some

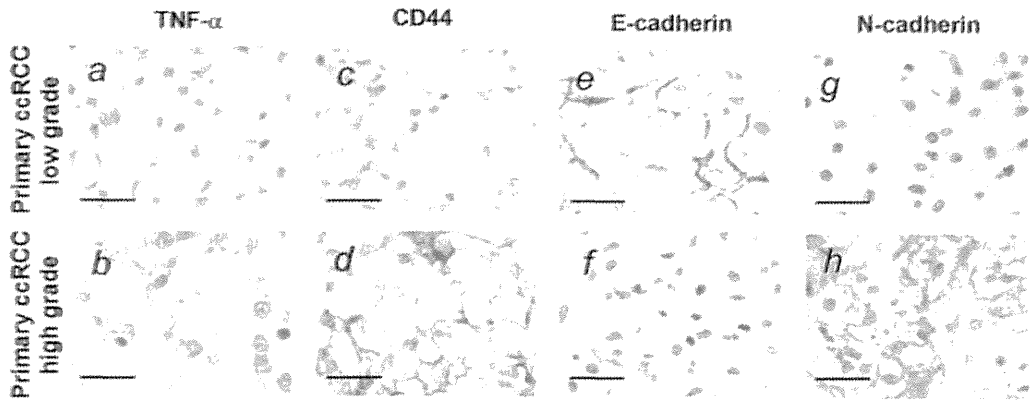

Figure 1. Expression of TNF-α, CD44, E-cadherin and N-cadherin in low-grade and high-grade primary ccRCCs. Paraffin sections were reacted with the antibodies against TNF-α (*a* and *b*) or CD44 (*c* and *d*), E-cadherin (*e* and *f*), N-cadherin (*g* and *h*). Bars, 25 μm.

cancer cells in low-grade ccRCCs were positive for E-cadherin staining (Fig. 1*e*), but most cancer cells in high-grade ccRCCs were negative (Fig. 1*f*). Cell surface N-cadherin staining was observed in 71% of the cases (85 of 120 ccRCCs). No apparent N-cadherin staining was observed in low-grade ccRCCs (Fig. 1*g*), but many cancer cells in high-grade ccRCCs showed positive staining (Fig. 1*h*). No immunoreaction was seen in negative controls incubated with non-immune mouse IgG or the antibodies absorbed with an excess amount of purified antigens (data not shown).

Correlations of TNF-α, CD44, E-cadherin and N-cadherin Expression with Clinicopathological Parameters in ccRCCs

TNF-α-positive cancer cell ratio varied from 0 to 100%, and its mean was 40%. As shown in Figures 2*a* to 2*c*, the ratio showed significant correlations with the parameters including pathological tumor stage ($p < 0.001$), distant metastasis ($p < 0.05$), and Fuhrman nuclear grade ($p < 0.001$). There was no significant association between the TNF-α-positive cancer cell ratio and lymph node metastasis (data not shown). CD44-positive cancer cell ratio ranged from 0 to 99%, and its mean was 11%. The ratio was positively correlated with pathological tumor stage ($p < 0.001$), and nuclear grade ($p < 0.001$; Figs. 2*d* and 2*f*). CD44-positive cancer cell did not associate with distant metastasis (Fig. 2*e*) or lymph node metastasis (data not shown). Co-upregulation of TNF-α and CD44 was associated with pathological tumor stage ($p < 0.001$), distant metastasis ($p = 0.036$) and Fuhrman nuclear grade ($p < 0001$; Supporting Information Table 2S).

E-cadherin positive cancer cell ratio ranged from 0 to 98%, and its mean was 18.4%. No significant association was observed between E-cadherin-positive cancer cell ratio and clinicopathological parameters (Supporting Information Table 3S). N-cadherin positive cancer cell ratio ranged from 0 to 91, and its mean was 27.8%. N-cadherin-positive cancer cell ratio was associated with pathological tumor stage ($p < 0.001$), lymph node metastasis ($p = 0.016$), and Fuhrman nuclear grade ($p < 0.001$; Supporting Information Table 3S). When ccRCCs were divided to TNF-α-high and TNF-α-low groups according to the TNF-α immunoreactive cell ratio, CD44-positive cancer cell ratio was significantly higher in TNF-α-high ccRCCs (17.2 ± 25.2) (mean ± SD) than in TNF-α-low ccRCCs (6.2 ± 16.4) ($p < 0.001$; Fig. 2*g*). There was no significant association between E-cadherin and TNF-α expression (Supporting Information Fig. 1S*a*) ($p = 0.992$). N-cadherin-positive cancer cell ratio was significantly higher in TNF-α-high ccRCCs (35.3 ± 27.7) than in TNF-α-low ccRCCs (19.0 ± 24.4) ($p < 0.001$) (Supporting Information Fig. 1S*b*).

Promotion of Migration, Invasion and CD44 Expression by Treatment of ccRCC Cells with TNF-α, and Effect of Hypoxia on TNF-α and CD44 Expression

When 786-O and ACHN ccRCC cells were treated with TNF-α, migration activity was significantly increased ($p < 0.05$; Fig. 3*a*). Similarly, TNF-α promoted Matrigel invasion of tumor cells ($p < 0.05$; Fig. 3*b*). Under the treatment with TNF-α, both cell lines showed decreased expression of E-cadherin mRNA ($p < 0.05$; Fig. 3*c*) and up-regulation of vimentin ($p < 0.05$; Fig. 3*d*), N-cadherin ($p < 0.01$; Fig. 3*e*), fibronectin ($p < 0.05$; Fig. 3*f*) and MMP9 mRNA ($p < 0.05$; Fig. 3*g*). Interestingly, TNF-α also increased TNF-α mRNA expression ($p < 0.01$; Fig. 3*h*). Immunoblot analysis revealed that TNF-α treatment down-regulated E-cadherin expression and up-regulated N-cadherin, vimentin and fibronectin at protein levels (Fig. 3*i*). TNF-α also up-regulates CD44 expression at both mRNA and protein levels in both 786-O and ACHN cells ($p < 0.05$; Figs. 4*a* and 4*b*). As shown in Figures 4*c* and 4*d*, culture of 786-O cells under hypoxic condition (1% oxygen) increased the mRNA expression of these molecules as compared with cells under normoxia (20% oxygen) ($p < 0.001$). 786-O cells treated with both TNF-α and hypoxia showed elevated TNF-α and CD44 expression compared to the cells

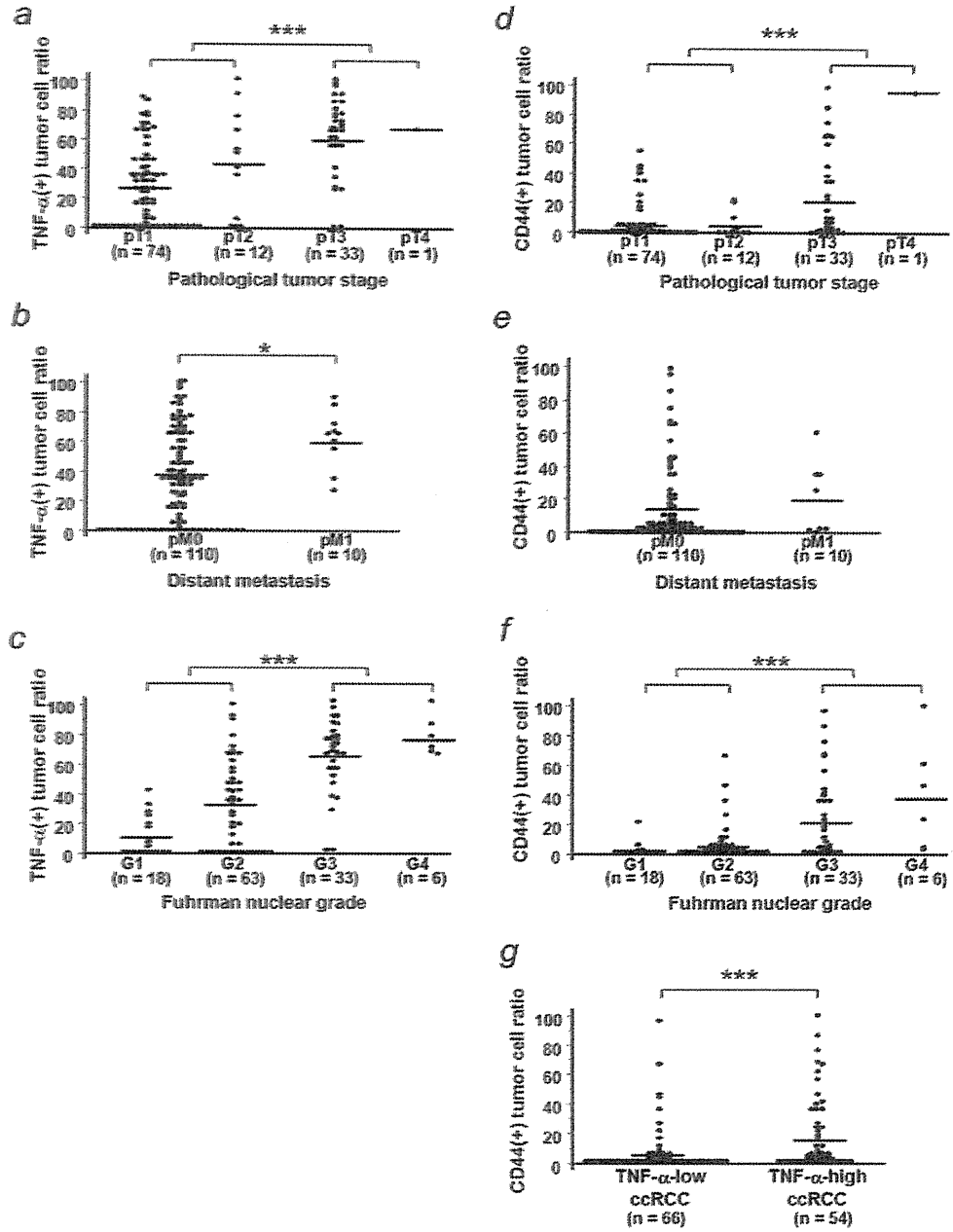

Figure 2. Correlations of TNF-α (*a–c*) and CD44 protein expression (*d–f*) with primary tumor stage, distant metastasis and Fuhrman nuclear grade, and CD44 expression levels in TNF-α-low or TNF-α-high ccRCCs (*g*) Bars, mean; $*p < 0.05$; $***p < 0.001$.

without treatment, but the degree of upregulation was similar to that with TNF-α treatment alone (Figs. 4*c* and 4*d*).

Correlations of TNF-α and CD44 Protein Expression with Prognosis of the ccRCC Patients

Immunohistologically, TNF-α protein expression was high in 55 patients and low in 65 patients, and patients with TNF-α-low tumor showed longer progression-free and overall survival rates than those with TNF-α-high tumor ($p < 0.001$; Figs. 5*a* and 5*b*). Expression of CD44 protein was high in 27 patients and low in 93 patients, and patients with CD44-low tumor exhibited longer progression-free and overall survival rates than those with CD44-high tumor ($p < 0.001$; Figs. 5*c* and 5*d*). When ccRCCs were classified into TNF-α-high/CD44-high, TNF-α-low/CD44-low, or other tumors, patients with TNF-α-high/CD44-high ccRCC showed dramatically

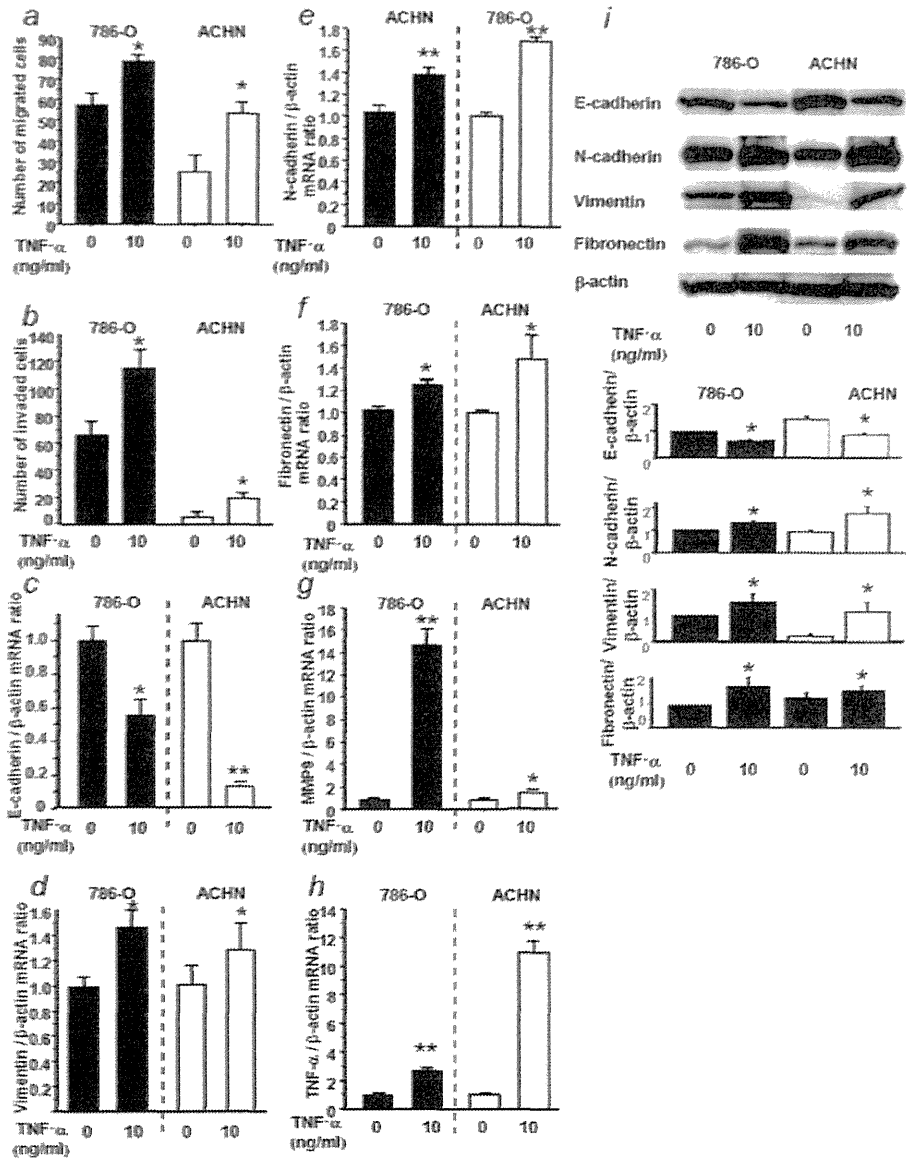

Figure 3. Effects of TNF-α on ccRCC cell lines. Changes in activities of migration (*a*) and invasion (*b*), mRNA expression of E-cadherin (*c*), vimentin (*d*), N-cadherin (*e*), fibronectin (*f*), MMP9 (*g*) and TNF-α (*h*) and protein expression of EMT markers (*i*) in ccRCC cell lines, after treatment with TNF-α. Gene expression levels are normalized to control samples' value to 1 for each cell lines. Columns, mean; Bars, SD; $*p < 0.05$; $**p < 0.01$.

worse progression-free survival compared to those with TNF-α-low/CD44-low tumors (Supporting Information Fig. 2Sa). All patients with TNF-α-low/CD44-low ccRCC were alive during follow-up (Supporting Information Fig. 2Sb).

Prognosis of the Patients Treated with Sunitinib and its Association with TNF-α and CD44 Expression

Among the 25 patients treated with sunitinib, TNF-α expression was high in 19 tumors and low in 6 tumors. Patients with TNF-α-high ccRCC showed relatively shorter time to treatment failure compared to those with TNF-α-low tumor, although the difference did not reach statistically significance ($p = 0.140$; Fig. 5*e*). All six patients with TNF-α-low tumor were alive during the follow-up periods, whereas 11 of 19 patients with TNF-α-high ccRCC died of the disease (Fig. 5*f*). CD44 expression was high in 8 and low in 17 tumors in 25 cases treated with sunitinib. Patients with CD44-high ccRCC had significantly shorter time to treatment failure and overall survival compared to those with CD44-low tumor ($p = 0.008$ and $p = 0.007$; Figs. 5*g* and 5*h*). Furthermore, patients with TNF-α-high/CD44-high ccRCC showed worse progression-free survival compared to those with TNF-α-low/

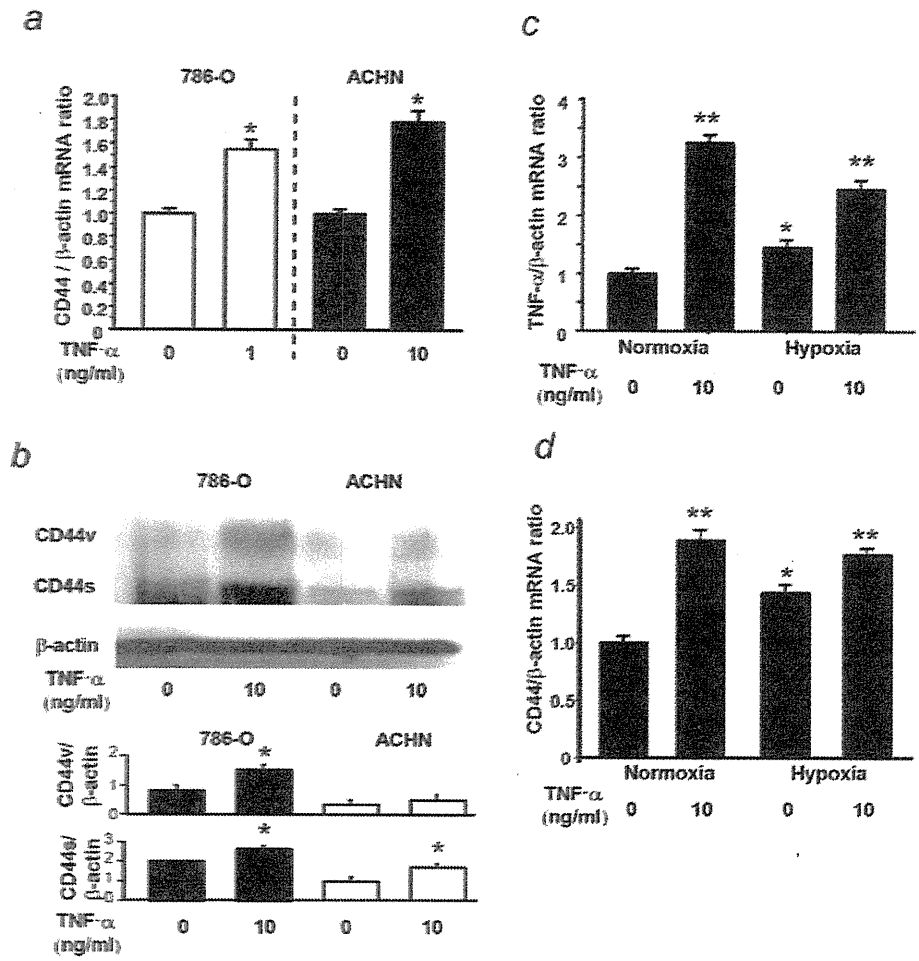

Figure 4. Effect of TNF-α on CD44 expression and effect of hypoxia on CD44 and TNF-α mRNA expression. Expression of CD44 mRNA and protein was examined by real-time PCR (*a*) and immunoblotting (*b*) after treatment with TNF-α. Protein expression of CD44 standard (CD44s) and CD44 variant forms (CD44v) was analyzed by densitometry of three independent experiments. TNF-α (*c*) and CD44 mRNA expression (*d*) under normoxia or hypoxia for 8 h was analyzed by quantitative real-time PCR. Gene expression levels are normalized to control samples' value to 1 for each cell lines. Columns, mean; Bars, SD; β-actin, a loading control; *$p < 0.05$; ***, $p < 0.001$.

CD44-low tumors ($p = 0.029$; Supporting Information Fig. 2S*c*). All patients with TNF-α-low/CD44-low ccRCC were alive during follow-up (Supporting Information Fig. 2S*d*). TNF-α expression in the ccRCCs of non-responders to the sunitinib treatment was slightly higher than that of responders (70.1 ± 50.4% *vs.* 50.4 ± 29.5%), although the difference did not reach statistically significance ($p = 0.127$). Similarly, tumors of non-responders to the sunitinib showed slightly higher CD44-positive cancer cell ratio (16.2 ± 20.8%) compared to those of responders (5.8 ± 13.9%) ($p = 0.134$).

Pathologic tumor stage, lymph node metastasis, distant metastasis, Fuhrman nuclear grade, TNF-α expression and CD44 expression were the prognostic factors for the progression-free and overall survivals by univariate analysis (Supporting Information Table 4S and 5S). Multivariate analysis revealed that Fuhrman nuclear grade ($p < 0.001$), TNF-α expression ($p = 0.008$) and CD44 expression ($p = 0.039$) were the independent prognostic factors for the progression-free survival (Supporting Information Table 4S). However, only Fuhrman nuclear grade was the independent prognostic factor for the overall survival ($p = 0.002$; Supporting Information Table 5S).

Finally, the significance of TNF-α and CD44 co-upregulation was evaluated by adjusting for the known prognostic factor, SSIGN.[18] In the SSIGN ≤ 3 category ($n = 7$), TNF-α and CD44 were significant predictors of progression-free and overall survivals (Supporting Information Figs. 3S*a* and 3S*b*). No patients with TNF-α-low/CD44-low ccRCC, whose tumors were SSIGN 4–7, showed tumor progression and died during follow-up (Supporting Information Figs. 3S*c* and 3S*d*). In the SSIGN ≥ 8 category, TNF-α/CD44 was no longer significant predictor of progression-free and overall survivals (Supporting Information Figs. 3S*e* and 3S*f*).

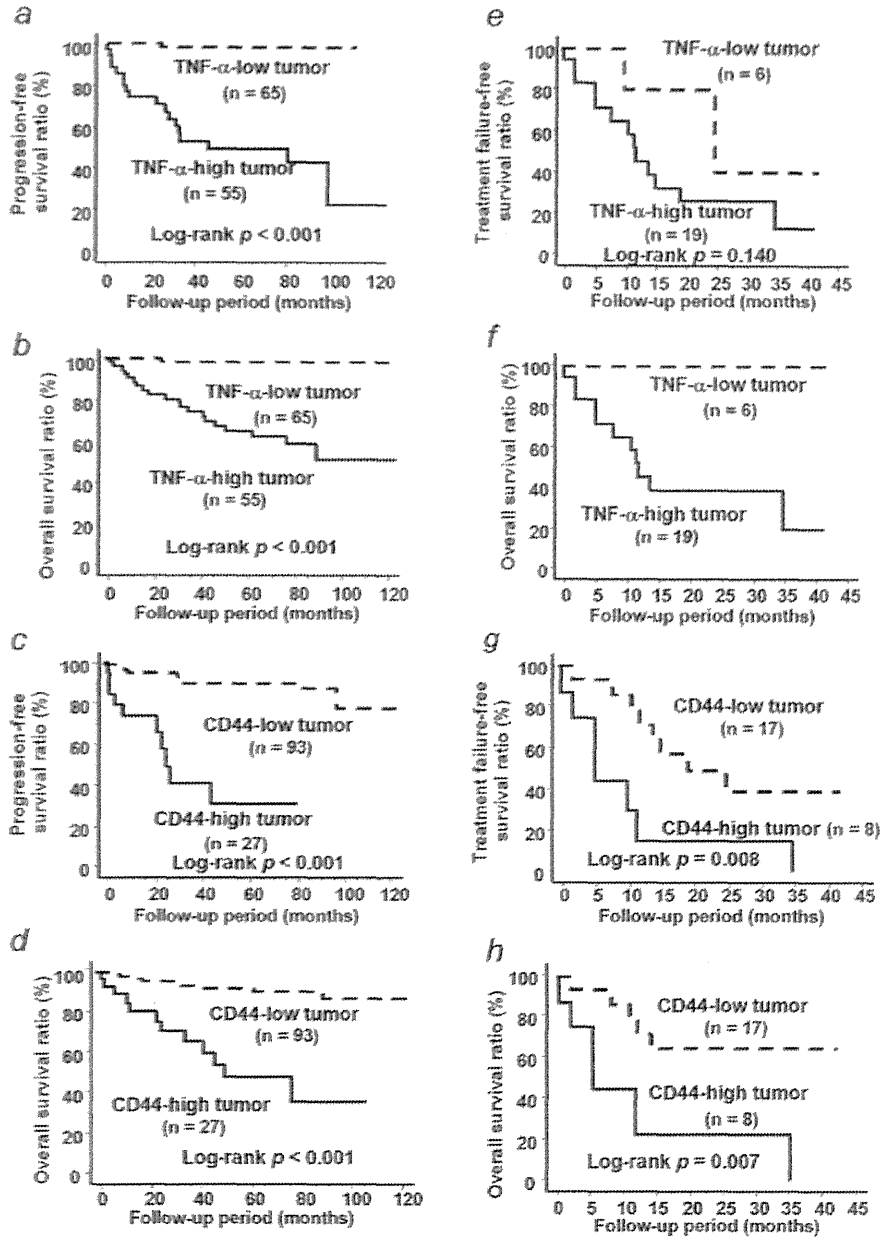

Figure 5. Kaplan-Meier curves of progression-free survival and overall survival according to the expression of TNF-α (*a* and *b*) and CD44 (*c* and *d*) in the 120 cases of ccRCC, and those of treatment-failure-free survival and overall survival according to the expression of TNF-α (*e* and *f*) or CD44 (*g* and *h*) in 25 ccRCCs treated with sunitinib. ccRCCs were classified into two groups according to TNF-α-low and TNF-α-high, or CD44-low and CD44-high cases as described in Materials and Methods.

Histology and Immunohistochemical Expression of TNF-α, CD44, E-cadherin and N-cadherin in Metastatic ccRCCs Removed from the Patients Treated or Untreated with Sunitinib

Metastatic ccRCCs without sunitinib treatment were composed of tumor cells located in a regular network of thin walled blood vessels (Fig. 6*a*), but the tumors with sunitinib treatment exhibited degeneration and necrosis of cancer cells (Fig. 6*b*). Both untreated and sunitinib-treated metastatic ccRCCs showed positive TNF-α staining (Figs. 6*c* and 6*d*). CD44 staining was observed in some cancer cells in untreated metastatic ccRCCs (Fig. 6*e*), while diffuse and strong staining was observed in residual tumor cells treated with sunitinib (Fig. 6*f*). E-cadherin staining was observed in some cancer

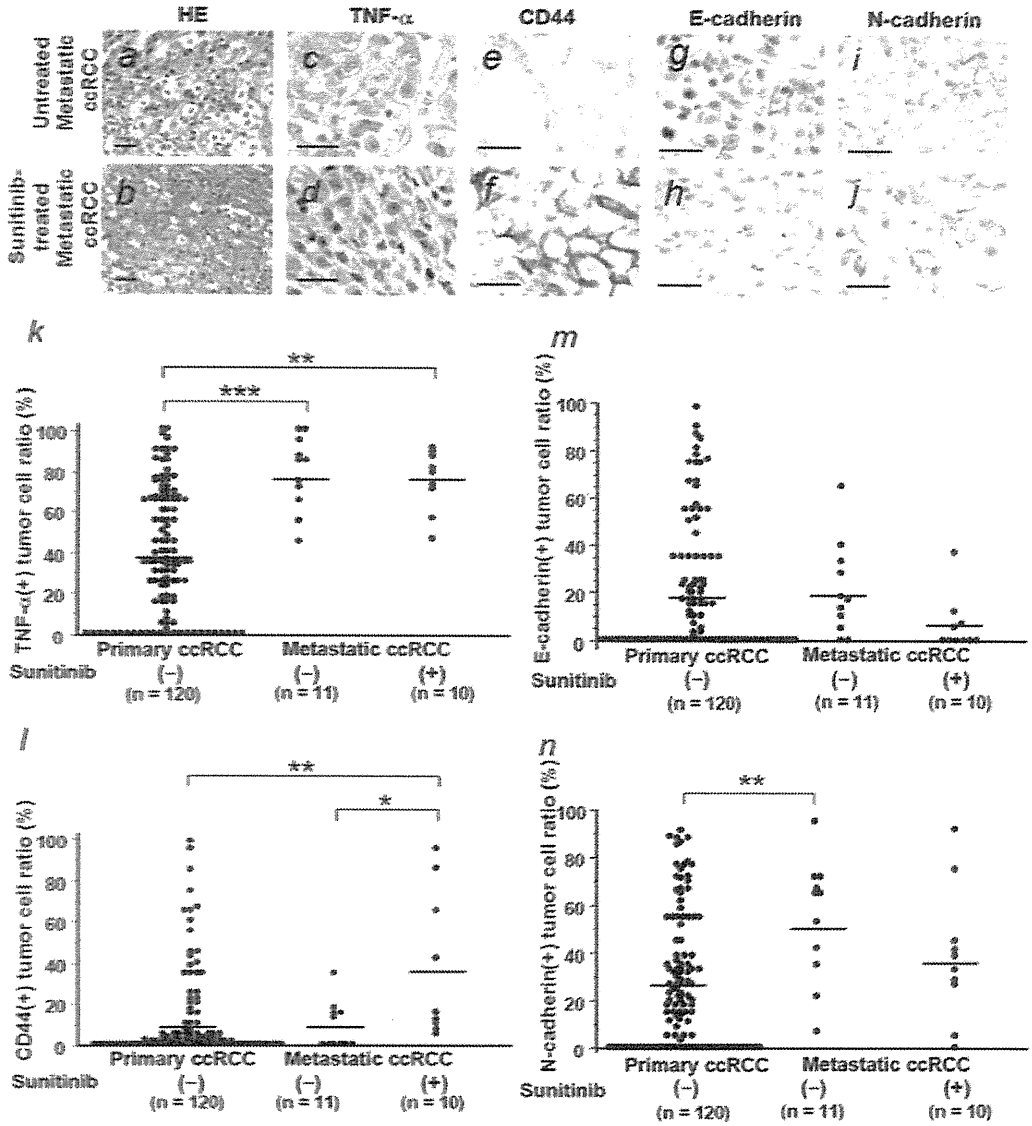

Figure 6. Staining of H&E (*a* and *b*), TNF-α (*c* and *d*) and CD44 (*e* and *f*), E-cadherin (*g* and *h*), and N-cadherin (*i* and *j*) in primary, untreated and sunitinib-treated metastatic ccRCCs, and differences in immunohistochemical expression of TNF-α (*k*), CD44 (*l*), E-cadherin (*m*) and N-cadherin (*n*) in untreated primary ccRCCs and metastatic ccRCCs untreated or treated with sunitinib. Bars in (*a*–*j*), 25 μm; bars in (*k*–*n*), mean; $*p < 0.05$; $**p < 0.01$; $***p < 0.001$.

cells in untreated metastatic ccRCCs (Fig. 6*g*), but it was almost lost in sunitinib-treated metastases (Fig. 6*h*). Both untreated and sunitinib-treated metastases showed diffuse N-cadherin staining (Figs. 6*i* and 6*j*).

TNF-α–positive tumor cell ratio was significantly higher in metastatic ccRCCs regardless of sunitinib treatment than in untreated primary tumors ($p < 0.001$ and $p < 0.01$; Fig. 6*k*). Logistic regression analysis also revealed that there was no significant association between TNF-α expression and sunitinib treatment ($R^2 = 0.003$, $p = 0.768$). CD44-positive tumor cell ratio was significantly higher in metastatic ccRCCs with sunitinib treatment than in untreated primary or metastatic tumors ($p < 0.01$ and $p < 0.05$; Fig. 6*l*). There was no significant difference between E-cadherin-positive tumor cell ratios in primary, untreated or sunitinib-treated metastatic ccRCCs (Fig. 6*m*). N-cadherin-positive tumor cell ratio was higher in untreated and sunitinib-treated metastatic ccRCCs than that in primary tumors ($p < 0.01$) (Fig. 6*n*).

Discussion

In the present study, we have demonstrated that the expression of TNF-α and CD44 in primary ccRCCs positively

correlates with pathological tumor stage, distant metastasis and histological grade. Studies using ccRCC cell lines have indicated that TNF-α suppresses E-cadherin expression and up-regulates MMP9 expression together with enhanced migration and invasion. Importantly, TNF-α up-regulates expression of CD44 and TNF-α itself. Multivariate analysis revealed that these were significant and independent predictors of progression-free survival. Furthermore, TNF-α-high/CD44-high ccRCCs showed dramatically worse prognosis compared to those with TNF-α-low/CD44-low tumors. Interestingly, sunitinib-treated metastatic ccRCCs showed high expression of TNF-α and CD44 in the tumor tissue. In addition, hypoxic treatment resulted in up-regulation of TNF-α and CD44 expression in ccRCC cells. All these data suggest that TNF-α has a key role in progression of ccRCCs by promoting EMT and may be involved in sunitinib resistance by induction of CD44.

Previous studies have indicated that TNF-α is overexpressed in many malignant neoplastic tissues, and proposed that the blood level of TNF-α may be a useful marker for the diagnosis and monitoring of some of such tumors including ccRCCs.[2,8,19,20] Our data revealed that TNF-α is predominantly overexpressed by carcinoma cells in high-grade ccRCC tissues as well as tumor-associated macrophages. TNF-α expression in ccRCC tissues positively correlated with primary tumor stage and distant metastasis, and showed inverse correlation with progression-free and overall survivals. Thus, TNF-α appears to play a key role in promotion of invasion and metastasis in ccRCCs. In fact, our *in vitro* study using ccRCC cell lines showed that TNF-α enhances invasion by induction of EMT and elevation of MMP9 expression. We have also demonstrated that TNF-α stimulates the ccRCC cells to produce TNF-α and increases the expression of CD44. These suggest that TNF-α acts as an up-stream molecule for the CD44 expression, and is involved in the overexpression of CD44 in the high-grade ccRCCs. It seems likely that ccRCCs have autocrine and paracrine pathways for TNF-α and CD44 expression within the ccRCC tissues, which were originally proposed in ovarian carcinomas.[3]

Previous studies have shown that median survival time is greater in the sunitinib-treated ccRCC patient group than in the interferon-α-treated group (26.4 months *vs.* 21.8 months),[10] and suggested that sunitinib contributes to inhibition of angiogenesis by blocking VEGF receptor kinase.[9] However, most of the sunitinib-treated patients die of the disease after all. Therefore, biomarkers that enable us to monitor the effect of sunitinib treatment and to select the most appropriate treatment are urgently needed to spare unnecessary toxicities and costs and to maximize the clinical benefit. Recent study on the patients with metastatic ccRCC after treatment with sunitinib has shown that blood levels of TNF-α and MMP9 are significantly increased in non-responders and associated with reduced progression-free and overall survivals.[20] The data are in accordance with our findings that the patients with TNF-α-high ccRCC had shorter survivals than those with TNF-α-low tumors. As shown in the previous and present studies, MMP9 expression is enhanced by treatment of ccRCC cells with TNF-α.[4] All these data suggest that TNF-α is a predictive biomarker for sunitinib efficacy and may be a target molecule for the treatment of the patients with metastatic ccRCC. Antibodies targeting TNF-α or its receptor have been clinically available for the treatment of rheumatoid arthritis and Crohn's disease,[21] and such antibodies have also been tested for metastatic ccRCC, showing partial responses and stabilization in some patients.[8] These results together with our findings in the current study provide the evidence that combined therapy of sunitinib and TNF-α blocking agent may be worth a clinical trial for the patients with metastatic ccRCC.

CD44 is known to be a potential cancer stem cell marker in various cancers.[7] The expression of CD44 is associated with chemotherapy-resistance in several cancers[7] and ablation of CD44 is known to enhance the effect of chemotherapeutic drugs in cancer cells.[22] These may explain the sunitinib resistance in the patients with advanced ccRCC. Molecular mechanism by which CD44 expression increases in the sunitinib-treated ccRCCs may be complex. TNF-α expression is negatively regulated by c-Jun NH_2-terminal kinase 1,[23] which is activated by PDGF,[24] and PDGF receptor inhibitor (AG1296) is known to enhance TNF-α secretion in leukemic cells.[25] Therefore, inhibition of PDGF receptor signals by sunitinib may increase TNF-α expression. On the other hand, hypoxia inducible factor-1α is reported to up-regulate the expression of both TNF-α and CD44 in hypoxic breast cancer cells[26] and cardiomyocytes.[27] In the present study, we also showed that hypoxic treatment up-regulates expression of TNF-α and CD44 in ccRCC cells. Since blocking of VEGF receptor signals in vascular endothelial cells by sunitinib seems to decrease the microvascularity in ccRCC tissues,[12] it may give focal hypoxia to ccRCC cells, leading to possible induction of TNF-α and CD44. In breast carcinomas, hypoxic region is known to contain cells with high-level expression of CD44.[26] Therefore, it is tempting to speculate that sunitinib treatment may have direct and/or indirect effects on carcinoma cells within the ccRCC tissues through induction of TNF-α, which then stimulates CD44 expression in ccRCC cells, finally leading to survival of cancer stem cell-like cells with high CD44 expression. Our data also suggest that therapy targeting TNF-α and/or CD44 may give a clue to improve the sunitinib-resistance in the ccRCC patients.

Acknowledgements

The authors thank Ms. Aya Shiraishi for her technical assistance. This work was supported in part by Grant-in-Aid for Scientific Research (C) (No.25460422), Grain-in-Aid for Scientific Research (S) (No. 26221005) from the Ministry of Education, Culture, Sports, Science, and Technology of Japan (MEXT) (S.M.), Grain-in-Aid for Scientific Research (B) (No. 24390374) from MEXT (M.O.), Project for Development of Innovative Research on Cancer Therapeutics (P-Direct) (S. M., R.M, K.T. and M.O.), and Grant-in-Aid for Scientific Research (A) (No. 24249022) from MEXT (Y.O.) and Third Term 10-year Strategy for Cancer Control from the Ministry of Health and Welfare (Y.O.).

References

1. Coussens LM, Werb Z. Inflammation and cancer. *Nature* 2002;420:860–7.
2. Balkwill F. Tumour necrosis factor and cancer. *Nat Rev Cancer* 2009;9:361–71.
3. Wu S, Boyer CM, Whitaker RS, et al. Tumor necrosis factor alpha as an autocrine and paracrine growth factor for ovarian cancer: monokine induction of tumor cell proliferation and tumor necrosis factor alpha expression. *Cancer Res* 1993; 53:1939–44.
4. Chuang MJ, Sun KH, Tang SJ, et al. Tumor-derived tumor necrosis factor-alpha promotes progression and epithelial-mesenchymal transition in renal cell carcinoma cells. *Cancer Sci* 2008;99:905–13.
5. Bhat-Nakshatri P, Appaiah H, Ballas C, et al. SLUG/SNAI2 and tumor necrosis factor generate breast cells with CD44+/CD24- phenotype. *BMC Cancer* 2010;10:411.
6. Muthukumaran N, Miletti-Gonzalez KE, Ravindranath AK, et al. Tumor necrosis factor-alpha differentially modulates CD44 expression in ovarian cancer cells. *Mol Cancer Res* 2006;4:511–20.
7. Zoller M. CD44: can a cancer-initiating cell profit from an abundantly expressed molecule? *Nat Rev Cancer* 2011;11:254–67.
8. Harrison ML, Obermueller E, Maisey NR, et al. Tumor necrosis factor alpha as a new target for renal cell carcinoma: two sequential phase II trials of infliximab at standard and high dose. *J Clin Oncol* 2007;25:4542–9.
9. Moldawer NP, Figlin R. Renal cell carcinoma: the translation of molecular biology into new treatments, new patient outcomes, and nursing implications. *Oncol Nurs Forum* 2008;35: 699–708.
10. Motzer RJ, Hutson TE, Tomczak P, et al. Overall survival and updated results for sunitinib compared with interferon alfa in patients with metastatic renal cell carcinoma. *J Clin Oncol* 2009;27: 3584–90.
11. Rini BI, Atkins MB. Resistance to targeted therapy in renal-cell carcinoma. *Lancet Oncol* 2009; 10:992–1000.
12. Griffioen AW, Mans LA, de Graaf AM, et al. Rapid angiogenesis onset after discontinuation of sunitinib treatment of renal cell carcinoma patients. *Clin Cancer Res* 2012;18:3961–71.
13. Greene FL BC, Fleming ID, et al. Kidney. In: Greene FL, Page DL, Fleming ID, Fritz A, Balch CM, Haller DG, Morrow M, eds. AJCC cancer staging handbook: TNM classification of malignant tumors, 6th edn. NY: Springer, 2002. 323–8.
14. Fuhrman SA, Lasky LC, Limas C. Prognostic significance of morphologic parameters in renal cell carcinoma. *Am J Surg Pathol* 1982;6:655–63.
15. Therasse P, Arbuck SG, Eisenhauer EA, et al. New guidelines to evaluate the response to treatment in solid tumors. European Organization for Research and Treatment of Cancer, National Cancer Institute of the United States, National Cancer Institute of Canada. *J Natl Cancer Inst* 2000;92:205–16.
16. Mikami S, Katsube K, Oya M, et al. Expression of Snail and Slug in renal cell carcinoma: E-cadherin repressor Snail is associated with cancer invasion and prognosis. *Lab Invest* 2011;91: 1443–58.
17. Shinojima T, Oya M, Takayanagi A, et al. Renal cancer cells lacking hypoxia inducible factor (HIF)–1alpha expression maintain vascular endothelial growth factor expression through HIF-2alpha. *Carcinogenesis* 2007;28:529–36.
18. Frank I, Blute ML, Cheville JC, et al. An outcome prediction model for patients with clear cell renal cell carcinoma treated with radical nephrectomy based on tumor stage, size, grade and necrosis: the SSIGN score. *J Urol* 2002;168: 2395–400.
19. Szlosarek P, Charles KA, Balkwill FR. Tumour necrosis factor-alpha as a tumour promoter. *Eur J Cancer* 2006;42:745–50.
20. Perez-Gracia JL, Prior C, Guillen-Grima F, et al. Identification of TNF-alpha and MMP-9 as potential baseline predictive serum markers of sunitinib activity in patients with renal cell carcinoma using a human cytokine array. *Br J Cancer* 2009;101:1876–83.
21. Wiedmann MW, Mossner J, Baerwald C, et al. TNF alpha inhibition as treatment modality for certain rheumatologic and gastrointestinal diseases. *Endocr Metab Immune Disord Drug Targets* 2009;9:295–314.
22. Tamada M, Nagano O, Tateyama S, et al. Modulation of glucose metabolism by CD44 contributes to antioxidant status and drug resistance in cancer cells. *Cancer Res* 2012;72:1438–48.
23. Peng T, Zhang T, Lu X, et al. JNK1/c-fos inhibits cardiomyocyte TNF-alpha expression via a negative crosstalk with ERK and p38 MAPK in endotoxaemia. *Cardiovasc Res* 2009;81:733–41.
24. Lopez-Ilasaca M, Li W, Uren A, et al. Requirement of phosphatidylinositol-3 kinase for activation of JNK/SAPKs by PDGF. *Biochem Biophys Res Commun* 1997;232:273–7.
25. Reiterer G, Bunaciu RP, Smith JL, et al. Inhibiting the platelet derived growth factor receptor increases signs of retinoic acid syndrome in myeloid differentiated HL-60 cells. *FEBS Lett* 2008; 582:2508–14.
26. Krishnamachary B, Penet MF, Nimmagadda S, et al. Hypoxia regulates CD44 and its variant isoforms through HIF-1alpha in triple negative breast cancer. *PLoS One* 2012;7:e44078.
27. Yu X, Deng L, Wang D, et al. Mechanism of TNF-alpha autocrine effects in hypoxic cardiomyocytes: initiated by hypoxia inducible factor 1alpha, presented by exosomes. *J Mol Cell Cardiol* 2012;53:848–57.

Nitric Oxide ■■ (2014) ■■–■■

Contents lists available at ScienceDirect

Nitric Oxide

journal homepage: www.elsevier.com/locate/yniox

Impacts of CD44 knockdown in cancer cells on tumor and host metabolic systems revealed by quantitative imaging mass spectrometry

Mitsuyo Ohmura [a], Takako Hishiki [a], Takehiro Yamamoto [a], Tsuyoshi Nakanishi [a,b], Akiko Kubo [a], Kenji Tsuchihashi [c,d], Mayumi Tamada [c], Sakino Toue [a], Yasuaki Kabe [a,e], Hideyuki Saya [c], Makoto Suematsu [a,e,*]

[a] Department of Biochemistry, Keio University School of Medicine, Tokyo 160-8582, Japan
[b] MS Business Unit, Shimadzu Corporation, Kyoto 604-8511, Japan
[c] Division of Gene Regulation, Institute for Advanced Medical Research, Keio University School of Medicine, Tokyo 160-8582, Japan
[d] Medicine and Biosystemic Science, Kyushu University Graduate School of Medical Sciences, Fukuoka 812-8582, Japan
[e] Japan Science and Technology Agency, Exploratory Research for Advanced Technology, Suematsu Gas Biology Project, Tokyo 160-8582, Japan

ARTICLE INFO

Article history:
Received 27 September 2014
Revised 5 November 2014
Accepted 9 November 2014
Available online

Keywords:
Remethylation
Transsulfuration
Reactive cysteine persulfides
Polyamines
xCT
Cancer

ABSTRACT

CD44 expressed in cancer cells was shown to stabilize cystine transporter (xCT) that uptakes cystine and excretes glutamate to supply cysteine as a substrate for reduced glutathione (GSH) for survival. While targeting CD44 serves as a potentially therapeutic stratagem to attack cancer growth and chemoresistance, the impact of CD44 targeting in cancer cells on metabolic systems of tumors and host tissues *in vivo* remains to be fully determined. This study aimed to reveal effects of CD44 silencing on alterations in energy metabolism and sulfur-containing metabolites *in vitro* and *in vivo* using capillary electrophoresis-mass spectrometry and quantitative imaging mass spectrometry (Q-IMS), respectively. In an experimental model of xenograft transplantation of human colon cancer HCT116 cells in superimmunodeficient NOG mice, snap-frozen liver tissues containing metastatic tumors were examined by Q-IMS. As reported previously, short hairpin CD44 RNA interference (shCD44) in cancer cells caused significant regression of tumor growth in the host liver. Under these circumstances, the CD44 knockdown suppressed polyamines, GSH and energy charges not only in metastatic tumors but also in the host liver. In culture, HCT116 cells treated with shCD44 decreased total amounts of methionine-pool metabolites including spermidine and spermine, and reactive cysteine persulfides, suggesting roles of these metabolites for cancer growth. Collectively, these results suggest that CD44 expressed in cancer accounts for a key regulator of metabolic interplay between tumor and the host tissue.

1. Introduction

Methionine is an essential amino acid provided by nutrition that starts remethylation cycle to synthesize S-adenosylmethionine (SAM), a donor metabolite necessary for transfer of methyl group to DNA and proteins, playing a critical role for epigenetic modification. SAM is also decarboxylated to yield polyamines including spermidine and spermine through methionine salvage pathway which plays a crucial role for regulation of cancer proliferation [1,2]. After donating methyl group, SAM is converted to S-adenosylhomocysteine (SAH) and then to homocysteine (Hcy) and methionine; these metabolites collectively form remethylation cycle, contributing to epigenetic regulation. A portion of Hcy that does not recycle to generate methionine is catalyzed by cystathionine β-synthase (CBS), the rate-limiting enzyme of transsulfuration pathway that generates cystathionine. This pathway plays a crucial role in ameliorating xenobiotic toxicity for cancer chemoresistance. Cystathionine γ-lyase (CSE), the 2nd enzyme of the pathway, catalyzes cystathionine to generate cysteine (Cys), providing a substrate for glutathione synthesis. Operation of methionine cycle and glutathione synthesis requires ATP.

Besides remethylation and transsulfuration pathways, the extracellular pathway dependent on CD44/xCT complex serves as an alternative mechanism to supply Cys to cells [3,4]. Through this mechanism in cancer cells, extracellular cystine (Cys-Cys) has been thought to enter cells to provide Cys for glutathione synthesis, so far as CD44 knockdown breaks down xCT stabilization and suppresses the entry of cystine and reduces GSH contents in cancer cells [4]. Previous studies revealed that Cys-Cys serves as a substrate for

* Corresponding author. Department of Biochemistry, Keio University School of Medicine, Tokyo 160-8582, Japan. Fax: +81 3 5363 3466.
E-mail address: gasbiology@z6.keio.jp (M. Suematsu).

http://dx.doi.org/10.1016/j.niox.2014.11.005
1089-8603/

Please cite this article in press as: Mitsuyo Ohmura, et al., Impacts of CD44 knockdown in cancer cells on tumor and host metabolic systems revealed by quantitative imaging mass spectrometry, Nitric Oxide (2014), doi: 10.1016/j.niox.2014.11.005

Table 1
Lists of metabolites with their theoretical and actual *m/z* values and MS^2 ion species in positive and negative ion mode.

Positive ion mode (Matrix: DHB)				
Compound name	Chemical formula	Monoisotopic molecular weight		Fragments observed in MS^2
		Theoretical	Actual	
		m/z	*m/z*	
SAM	$C_{15}H_{23}N_6O_5S$	399.145	399.141	250.093, 298.096, 136.064
SAH	$C_{14}H_{20}N_6O_5S$	385.129	385.126	250.087, 136.063, 134.027
Spermidine	$C_7H_{19}N_3$	146.166	146.155	129.027, 72.058, 112.088
Spermine	$C_{10}H_{26}N_4$	203.224	203.212	129.139,112.104, 84.082
Adenosine	$C_{10}H_{13}N_5O_4$	268.105	268.086	136.059
Negative ion mode (Matrix: 9AA)				
Compound name	Chemical formula	Monoisotopic molecular weight		Fragments observed in MS^2
		Theoretical	Actual	
		m/z	*m/z*	
UDP-HexNAc	$C_{17}H_{27}N_3O_{17}P_2$	606.074	606.068	385.031, 403.030, 282.039, 272.954, 323.046, 305.018, 362.055
GSH	$C_{10}H_{17}N_3O_6S$	306.076	306.067	254.087, 179,050, 272.072, 143,048, 159.932, 210.092, 128.030, 171.032
GSSG	$C_{20}H_{32}N_6O_{12}S_2$	611.144	611.137	306.071, 272.086, 338.058, 254.079, 482.103, 304.058, 288.058, 593.121
GSO_3^-	$C_{10}H_{17}N_3O_9S$	354.061	354.038	179.036, 336.099, 225.006, 210.075, 135.050, 254.062, 193.063, 143.031, 261.002
$GSSO_3^-$	$C_{10}H_{17}N_3O_9S_2$	386.033	386.008	306.058, 179.036, 254.062, 272.071, 288.049, 368.000, 160.000, 143.040, 210.076, 194.050
ATP	$C_{10}H_{16}N_5O_{13}P_3$	505.988	505.986	408.046, 272.955, 158.924, 176.934
ADP	$C_{10}H_{15}N_5O_{10}P_2$	426.022	426.032	328.070, 134.048
AMP	$C_{10}H_{14}N_5O_7P$	346.055	346.094	210.998, 149.988, 192.991, 134.041
Gln	$C_5H_{10}N_2O_3$	145.061	145.060	127.053, 109.042
Glu	$C_5H_9NO_4$	146.045	146.047	128.022, 102.046
Taurine	$C_2H_7NO_3S$	124.007	124.010	79.958, 106.978
Asp	$C_4H_7NO_4$	132.030	132.031	88.038, 115.013
Malate	$C_4H_6O_5$	133.014	133.015	115.006, 71.018

SAM: S-Adenosyl-L-methionine, SAH: S-Adenolsyl-L-homocysteine, UDP-HexNAc: UDP-N-acetyl hexosamine, GSH: Glutathione, reduced form, GSSG: Glutathione oxidized form, GSO_3^-: Glutathione sulfonate, $GSSO_3^-$: Glutathione S-sulfonate.

CBS and CSE to generate cysteine hydropersulfide (Cys-SSH) as a primary product of these enzymes. This reactive persulfide can react with reduced glutathione (GSH) to form glutathione hydropersulfide (GSSH) and other derivatives including cysteine-glutathione disulfide (Cys-SSG) and hydrogen sulfide anion (HS^-) and other polysulfide derivatives of thiol-containing peptides and proteins [5]. Compared with glutathione and hydrogen sulfide, Cys-SSH derivatives were superior nucleophiles and reductants and capable of detoxifying nucleophiles [5], benefiting amelioration of oxidative stress in cancer cells.

Since methionine and cysteine might be derived from host tissues during cancer development, it is not unreasonable to hypothesize that CD44 targeting by RNA interference or small molecular reagents does not only contribute to cancer regression but also alter metabolic systems of the host tissues. We have recently developed quantitative imaging mass spectrometry (Q-IMS) as a novel method to collect quantitative information of many metabolites in tumor-bearing tissues. Using this technique combined with super-immunodeficient mice for xenograft transplantation of human-derived cancer cells, the current study aimed to examine influence of CD44 knockdown in human-derived colon cancer HCT116 cells on metabolic systems in metastatic tumors and the liver as a host tissue. The results showed that the CD44 knockdown suppressed polyamines, GSH and energy charges not only in metastatic tumors but also in the host liver, suggesting that CD44 in cancer cells support the metabolic interplay between tumors and the host tissue, benefiting cancer proliferation and survival.

2. Materials and methods

2.1. Stable CD44 interference with shRNA

Using expression vectors encoding a shRNA specific for human CD44 mRNA or a scrambled shRNA obtained from Origene Technologies (Rockville, MD), we introduced it into HCT 116 cells by transfection with Lipofectamine 2000 [4]. The sequence of shRNA used for CD44 knockdown (shCD44) throughout all studies was 5'-GCTGACCTCTGCAAGGCTTTCAATAGCAC-3'. The control non-targeting shRNA sequence was 5'-GCACTACCAGAGCTAACTCAGATAGTACT-3', designated as control shRNA unless otherwise mentioned.

2.2. Human-derived cancer xenografts in livers of superimmunodeficient mice

All animal experiments were carried out in accordance with the guidelines of Experimental Animal Committee of Keio University School of Medicine. Human colon cancer (HCT116) cells were transfected stably with non-target control shRNA or with shCD44. The cells were injected into the spleen of superimmunodeficient NOG (NOD/SCID/IL-2Rγ^{null}) mice as described previously [6–8]. In brief, HCT116 cells were injected into the spleen of male NOG mice aged at 11~14 weeks at 1×10^6 cells/mouse. Two weeks after transplantation, liver lobules of the mice fasted for 17 hours were excised under sevoflurane anesthesia and snap-frozen with liquid nitrogen. To examine tumor growth *in vivo*, 5-μm thickness cryosections were stained with hematoxylin and eosin (H&E), serving as

Please cite this article in press as: Mitsuyo Ohmura, et al., Impacts of CD44 knockdown in cancer cells on tumor and host metabolic systems revealed by quantitative imaging mass spectrometry, Nitric Oxide (2014), doi: 10.1016/j.niox.2014.11.005

Table 2
Composition of culture medium used in the study (g/L).

	DMEM-(A)	DMEM-(B)	DMEM-(C)
Amino acids			
L-Alanine	0.00445	0.00445	0.0356
L-Arginine·HCl	0.1475	0.1475	0.084
L-Asparagine·H_2O	0.0075	0.0075	0.06
L-Aspartic acid	0.00665	0.00665	0.0532
L-Cystine·2HCl	0.03129	0.01756	
L-Cysteine·HCl·H_2O	0.01756	0.03129	
L-Glutamic acid	0.00735	0.00735	0.0588
L-Glutamine	0.365	0.365*	0.584
Glycine	0.01875	0.01875	0.03
L-Histidine·HCl·H_2O	0.03148	0.03148	0.042
L-Isoleucine	0.05447	0.05447	0.105
L-Leucine	0.05905	0.05905*	0.105
L-Lysine·HCl	0.09125	0.09125*	0.146
L-Methionine	0.01724	0 or 0.01724**	0.03
L-Phenylalanine	0.03548	0.03548	0.066
L-Proline	0.01725	0.01725	0.046
L-Serine	0.02625	0.02625	0.042
L-Threonine	0.05345	0.05345	0.095
L-Tryptophan	0.00902	0.00902	0.016
L-Tyrosine·2Na·2H_2O	0.05579	0.05579	0.104
L-Valine	0.05285	0.05285	0.094
Inorganic salts			
$CaCl_2$·2H_2O	0.1545	0.1545*	
$CaCl_2$·9H_2O			0.265
$CuSO_4$·5H_2O	0.0000013	0.0000013	
$Fe(NO_3)_3$·9H_2O	0.00005	0.00005	0.0001
$FeSO_4$·7H_2O	0.000417	0.000417	
$MgCl_2$·6H_2O	0.0612	0.0612*	
$MgSO_4$	0.04884	0.04884*	0.09767
KCl	0.3118	0.3118	0.4
NaCl	6.996	6.996	4.75
$NaHCO_3$	1.2	1.2*	3.7
Na_2HPO_4	0.07102	0.07102	
NaH_2PO_4	0.0543	0.0543	0.109
$ZnSO_4$·7H_2O	0.000432	0.000432	
Vitamins			
D-Biotin	0.0000035	0.0000035	
Choline chloride	0.00898	0.00898	0.004
Folic acid	0.00266	0.00266	0.004
myo-Inositol	0.0126	0.0126	
i-Inositol			0.0072
Niacinamide	0.00202	0.00202	0.004
D-Pantothenic acid·1/2Ca	0.00224	0.00224	0.004
Pyridoxal·HCl	0.002	0.002	
Pyridoxine·HCl	0.002031	0.000031	0.004
Riboflavin	0.000219	0.00219	0.0004
Thiamine·HCl	0.00217	0.00217	0.004
Vitamin B_{12}	0.00068	0.00068	
Others			
D-Glucose	3.15	3.15	3.15
HEPES		3.5745	5.958
Hypoxanthine	0.00244	0.0021	
Linoleic acid	0.000042	0.000042	
Putrescine·2HCl	0.000081	0.000081	
Pyruvic acid·Na	0.055	0.055	
DL-Thioctic acid	0.000105	0.000105	
Thymidine	0.000365	0.000365	
Phenol red	0.00863		0.01493

DMEM-(A): DMEM F-12 (Sigma-Aldrich, D8062), DMEM-(B): DMEM F-12(Sigma-Aldrich, D9785), DMEM-(C): modified DMEM.

* As DMEM F-12 does not contain these components, these are added when the medium is prepared.

** Experiments determining effects of the presence and absence of methionine were performed using DMEM-(B).

resources of microscopic images for calculating cross-sectional percentages of tumor regions with Image J software [9].

2.3. Quantitative imaging mass spectrometry (Q-IMS)

Snap-frozen tissues collected from the non-targeting control- or shCD44-transfected HCT116 cell-derived tumor-bearing livers were used for, Q-IMS according to our previous methods [7,10,11,12]. Briefly, as a matrix, 5 mg/mL 9-aminoacridine (Merck Schucardt, Hohenbrunn, Germany) in 80% ethanol solution was sprayed over the 5-μm thickness liver sections which were thaw-mounted on ITO-coated glass slides (Bruker Daltonik GmbH, Bremen, Germany). MALDI IT-TOF mass spectrometer (Shimadzu Corp., Kyoto, Japan) allowed us to collect the data in the negative ion mode with the recording mass range from *m/z* 304 to 670. After selecting the region of interests (ROIs) by light microscopic observations, a series of repeated laser irradiation at 100 times per spot was performed at 10-μm pitch intervals at 250 × 250 spots, giving 62,500 data points in total for each scan. Averaged spectra from each ROIs were generated and statistically analyzed by house-made software SIMtools (Shimadzu Imaging Mass spectrometry toolbox for MATLAB®) as described previously. To evaluate small molecules such as amino acids, we performed the measurement with the mass range of *m/z* 86–400 at 25-μm intervals at 100 × 100 spots. Mass peaks of metabolites collected from tissue sections were identified by comparing MS/MS fragment patterns with those collected from standard reagents (Table 1).

CE-MS analyses allowed us to determine contents of varied metabolites in a portion of tumor-bearing liver tissues which was adjacent to the corresponding IMS section as described previously [7,10,12]. To calculate the apparent contents in parenchymal and tumor regions of tumor-bearing livers ($[C_p]_{app}$ and $[C_T]_{app}$, respectively), the following equations were used after calculating cross-sectional percentage areas of tumor regions (O_T %) that are calculated in digital tissue images collected from H&E stained sections as described elsewhere:

$$I_{Average} = (I_P \times O_P)/100 + (I_T \times O_T)/100, O_P + O_T = 100\,(\%) \quad (1)$$

$$[C_T]_{app} = [C_{CE\text{-}MS}] \times (I_T / I_{Average}) \quad (2)$$

$$[C_p]_{app} = [C_{CE\text{-}MS}] \times (I_p / I_{Average}) \quad (3)$$

$$C_i = [C_{CE\text{-}MS}] \times (I_{(i)} / I_{Average}) \quad (4)$$

I_T, I_p and $I_{Average}$ are MALDI signal intensities measured in regions of tumor metastases, liver parenchyma and the whole tissue section, respectively. O_T and O_p are the percentage areas of tumor regions and liver parenchymal regions, respectively. In order to calculate the values of $[C_T]_{app}$ and $[C_p]_{app}$, we used the equation (2) from 2–4 sets of IMS data paired with CE-MS data for individual mice in each group. To construct an ion-content map, MALDI-MS data were converted to Analyze format, a common multidimensional biomedical imaging format file which contains MALDI signal intensity at each pixel I(*i*), and equation (4) was used to calculate the apparent contents of metabolites of interest at each pixel "*i*" (*Ci*).

We attempted to visualize methionine-derived metabolites such as S-adenosylmethionine (SAM), S-adenosylhomocysteine (SAH), spermidine and spermine using 30 mg/mL 2,5-dihydroxybenzoic acid (DHB) in 70% methanol solution as a matrix for positive-mode MALDI [11]. To avoid influence of the noise induced by DHB, we measured with the scanning mass range of *m/z* 140–300 and *m/z* 350–500 at 25-μm intervals at 100 × 100 spots.

In separate sets of experiments, glutathione sulfonate (GSO_3^-) and glutathione S-sulfonate ($GSSO_3^-$) were measured. As described previously, GSO_3^- is a terminal oxidized product yielded from glutathione. On the other hand, $GSSO_3^-$ is a terminal oxidized product yielded in the presence of H_2S/HS^- under atmospheric MALDI conditions [10], serving as an index of endogenous persulfide generation. In these experiments, we did not calculate $[C_{CE\text{-}MS}]$ and *Ci*, because their generation rates are different between CE-MS and MALDI imaging. Instead, the data of GSO_3^- and $GSSO_3^-$ were evaluated by

Please cite this article in press as: Mitsuyo Ohmura, et al., Impacts of CD44 knockdown in cancer cells on tumor and host metabolic systems revealed by quantitative imaging mass spectrometry, Nitric Oxide (2014), doi: 10.1016/j.niox.2014.11.005

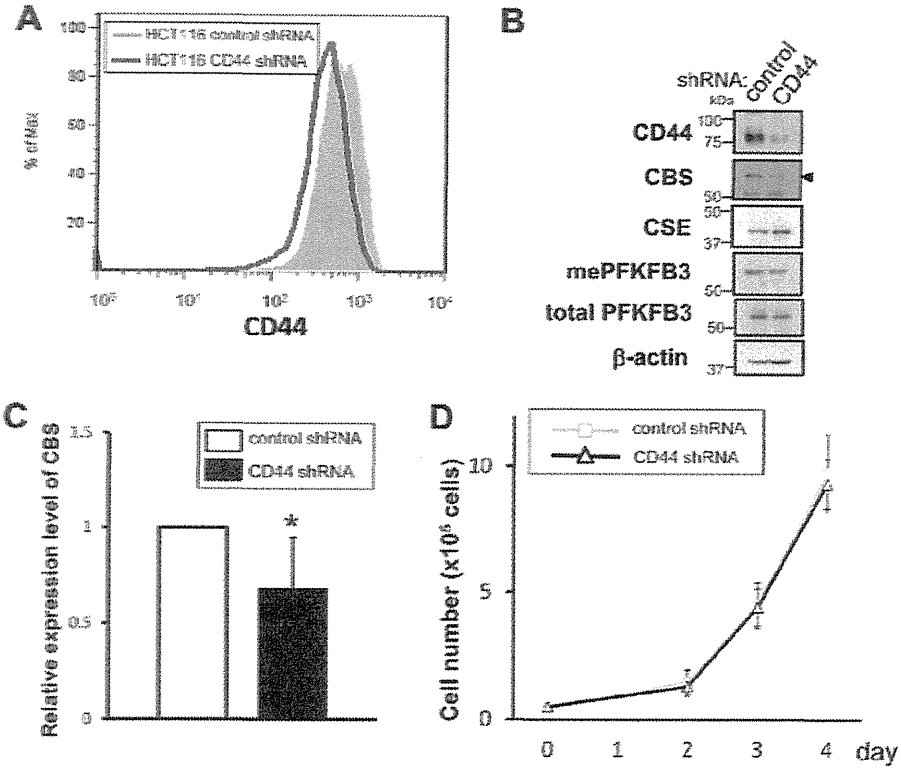

Fig. 1. Effects of CD44 knockdown on thiol-metabolizing enzymes and cell proliferation. A. Flow cytometric analysis of CD44 expression on HCT116 cells transfected with control or CD44 shRNAs. B. Effects of CD44 knockdown on thiol-metabolizing enzymes. Lysates were analyzed by immunoblotting with anti-CD44, anti-CBS, anti-CSE, anti-PFKFB3 and anti-dimethyl-PFKFB3 (R131/134) antibodies. The expression of level of β-actin was used as a loading control. Arrowhead indicates CBS-specific bands. C. Densitometric analysis of CBS protein expression levels. Data indicate the values of relative expression level of CBS (mean ± SD, n = 6); $^{*}p < 0.05$ versus control shRNA with unpaired Student's *t*-test. D. Effects of CD44 knockdown on proliferation of HCT116 cells. The cells were seeded in each well (5×10^4 cells/well) and cell numbers were counted at 48, 72 and 96 hours after inoculation. Open squares and triangles indicate data from control and CD44-silencing cells, respectively. Data represent mean ± SD of 6 separate experiments. $^{*}p < 0.05$ versus the HCT116 cells with control shRNA (ANOVA with Fisher's multiple comparison test).

measuring their mass peaks. These experiments were carried out using a negative mode in the presence of 9-aminoacridine as a matrix reagent.

Compositions of culture medium used for the current study were described in Table 2. DMEM-(A) was a standard culture medium (DMEM F-12, Sigma-Aldrich) used for culturing HCT116 cells in the atmospheric conditions (95% Air / 5% CO_2) at 37 °C. DMEM-(B) was the methionine-free DMEM F-12 available from Sigma-Aldrich. DMEM-(C) was used to examine effects of the absence of cystine and cysteine in the culture. DMEM-(C) was a generous gift from Ajinomoto Co., Inc. (Kawasaki City, Japan). In these experiments, 0.02403 g/L of L-cystine, that is comparable to cystine contents in DMEM-(A), was added to DMEM-(C), and used for the control experiments. Unless otherwise mentioned, DMEM-(A) was used as a standard culture medium for experiments *in vitro*.

2.4. Measurements of monobromobimane adducts to assess reactive cysteine persulfides

For culture experiments, 2×10^4 HCT116 cells treated with non-target shRNA or those with shCD44 were cultured in 5% CO_2 at 37 °C in DMEM F-12 medium (Sigma-Aldrich, St Louis, MO) supplemented with 10% fetal bovine serum and 1% penicillin-streptomycin (Invitrogen, Carlsbad, CA) for 48 hrs, and used for viability study in the presence or absence of different concentrations of methionine and/or propargylglycine (PPG, Sigma-Aldrich, US), a potent inhibitor of cystathionine γ-lyase (CSE) [13,14]. The cell viability was examined by Cell Counting Kit-8 (CCK-8 kit) (Dojindo Laboratories, Kumamoto, Japan). When necessary, the cells were frozen and thawed to measure metabolites using capillary electrophoresis-mass spectrometry (CE-MS) as described previously [15]. In separate sets of experiments under the identical protocols, we determined reactive cysteine persulfides using LC-MS/MS supported by monobromobimane derivatization method [16]. Briefly, cells in culture were washed with PBS twice and plunged into methanol containing 50 nM D-camphor-10-sulfonic acid (CSA) as an internal standard. Cell extracts and cultured medium were collected and the samples were thoroughly mixed with 0.5 mL deionized water and 1 mL chloroform, and centrifuged at 12,000 *g* for 15 min at 4 °C. The upper aqueous phase was filtered through a 5-kDa cutoff filter (Ultrafree-MC UFC3LCC; Millipore, Billerica, MA) to remove protein precipitates. After the lyophilization of filtrates, the precipitates were dissolved in 50 μL deionized water. Subsequently, the samples were incubated with 2 mM monobromobimane (MBB) on ice for 5 min. Because of its insolubility, MBB was predissolved in a minimum volume of DMSO. MBB derivatives in the cell extracts were determined using a Nexera UHPLC system coupled with an LCMS-8030 triple quadrupole mass spectrometer (Shimadzu, Kyoto, Japan) as an LC-MS/MS instrument. Separation was achieved on a C18 reversed-phase column (ACQUITY CSH C18, 1.7 μm, 2.1 × 150 mm; Waters, Milford, MA) with a pre-column (ACQUITY UPLC CSH C18 VanGuard, 1.7 μm, 2.1 × 5 mm; Waters). The MBB derivatives were eluted with acetonitrile gradients containing 0.1% formic acid: 5% CH_3CN for 2.5 min, gradient to 13% CH_3CN for 2.5 min, gradient to 20% CH_3CN for 4 min, gradient to 50% CH_3CN for 30 sec, gradient to 98% CH_3CN for 3 min, and held for 2.5 min. The injection volume

Please cite this article in press as: Mitsuyo Ohmura, et al., Impacts of CD44 knockdown in cancer cells on tumor and host metabolic systems revealed by quantitative imaging mass spectrometry, Nitric Oxide (2014), doi: 10.1016/j.niox.2014.11.005

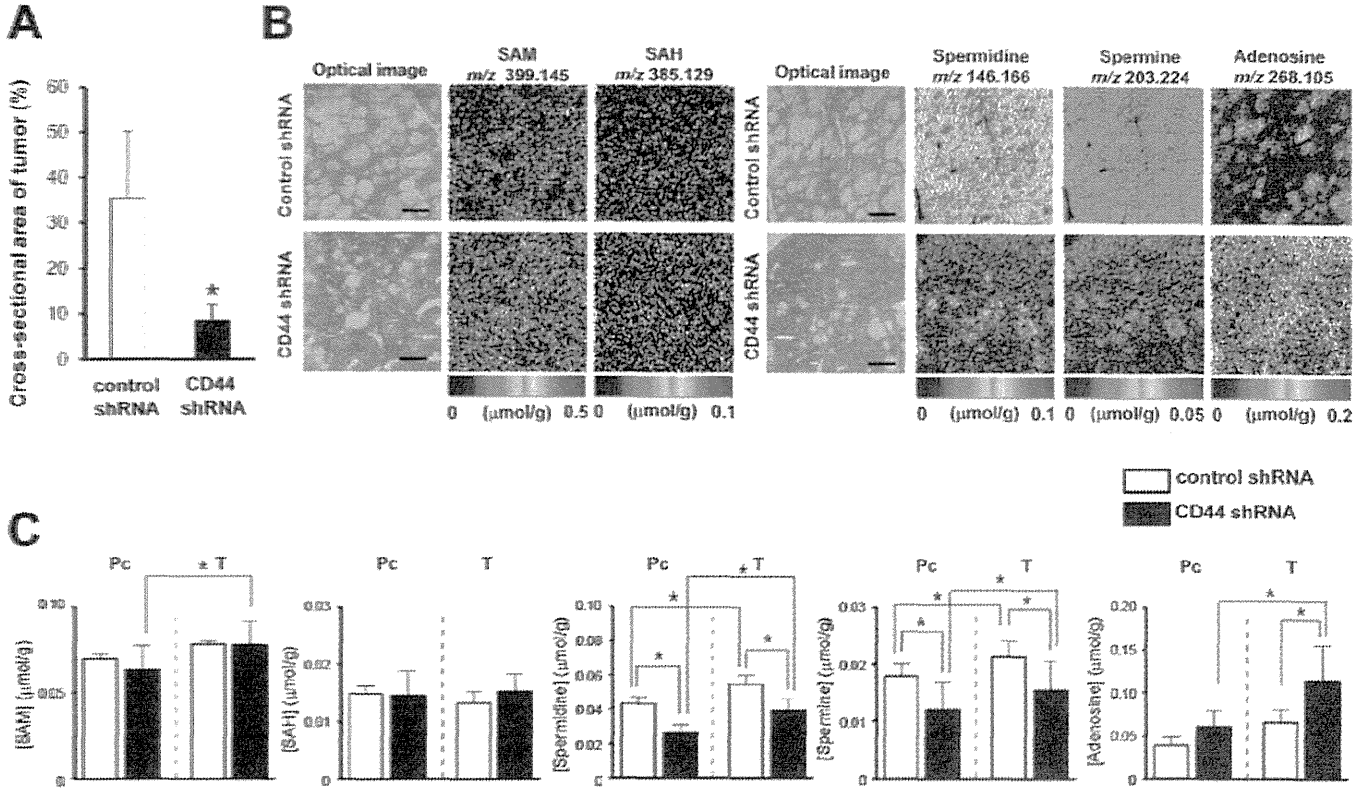

Fig. 2. CD44 knockdown alters contents of spermine and spermidine in tumors and host liver. A. Decrease of cross-sectional area of tumors in which CD44 shRNA cells were transplanted for 2 weeks. Data indicate mean ± SD of 4–6 mice for each group. $^*p < 0.05$ versus control shRNA with unpaired Student's *t*-test. B. CD44 induced decrease of spermidine and spermine in both liver parenchyma and metastatic tumors. By positive-mode quantitative IMS with the resolution of 25-μm intervals at 100 × 100 spots, cationic metabolites were measured using mass microscope. To maintain the detection sensitivity of ions, we measured with 2 different scanning mass ranges separately: *m/z* 350–500 and *m/z* 140–300. Left panels are optical images which were obtained before IMS measurements. Color bar and associated numbers under images indicate apparent amounts of metabolites expressed as μmol/g tissue. Scale bar: 500 μm. The *m/z* values for determining individual metabolites follow those indicated in Table 1. C. Quantitative determination of apparent contents metabolites in liver parenchyma (Pc) and tumor regions (T) which control shRNA or CD44 shRNA cells were tranplanted for 2 weeks. $^*p < 0.05$. Values indicate apparent amounts of metabolites expressed as μmol/g tissue. Data indicate mean ± SD of 4–6 mice for each group. ANOVA with Fisher's multiple comparison test was used.

was 10 μL. Column oven was kept at 40 °C and the flow rate was set to 0.25 mL/min. Optimization of multiple reaction monitoring (MRM) transition for the MBB derivatives was automatically performed by the built-in algorithm of the LCMS-8030; and the optimized MRM transitions were *m/z* 413.10 > 191.15 for sulfide-dibimane (SDB) on negative mode, *m/z* 326.10 > 193.15 for homocysteine-bimane (Hcy-bimane), *m/z* 358.10 > 192.00 for homocysteine persulfide-bimane (Hcy-S-bimane), *m/z* 344.15 > 223.00 for cysteine persulfide-bimane (Cys-S-bimane), and *m/z* 530.20 > 191.95 for glutathione persulfide-bimane (GS-S-bimane) in positive mode. The transition of CSA was monitored for *m/z* 231.10 > 80.10 in negative mode. Retention time was considered using the standard of the derivatives according to the LC condition described above. The interface ionization potential was set at 4.5 kV with a temperature of 400 °C. The flow rates of nebulizer and drying gases were set at 1.5 and 10 L/min, respectively. The standard reagents of MBB derivatives were purchased from Shinsei Chemical (Osaka, Japan).

2.5. Western blotting

Cell extracts were mixed with equivalent volume of 2× Laemmli sample buffer (62.55 mM Tris-HCl; pH6.8, 2% SDS, 25% Glycerol, and 0.01% Bromophenolblue) with or without (for the detection of CD44) 10% (w/v) 2-mercaptoethanol. The equivalent amounts of proteins (25 μg/lane) were separated by 10% SDS-PAGE and transferred onto PVDF membranes. The membranes were blocked in PBST (0.15 M NaCl, 10 mM Tris-HCl; pH7.5, and 0.1% Tween20) containing 3% (w/v) skim milk for 1 h at room temperature. Subsequently, the membranes were probed with the primary antibody for overnight at 4 °C. Following the incubation of primary antibodies, the membranes were incubated with the appropriate HRP-conjugated secondary antibody for 2 h at room temperature. Signals were visualized by ECL Prime (GE Healthcare, Amersham, UK).

The following primary antibodies were used in Western blotting: anti-CD44 mouse monoclonal (ab6124, Abcam, Cambridge, UK; 3,000× dilution), anti-CSE mouse monoclonal (H00001491-M03, Abnova, Taipei, Taiwan; 7,000× dilution), anti-CBS mouse monoclonal (H00000875-M01, Abnova; 7,000× dilution), anti-beta actin mouse monoclonal (A1978, Sigma-Aldrich, St. Louis, MO; 10,000× dilution), anti-PFKFB3 mouse monoclonal (H00005209-M08, Abnova; 2,000× dilution), and anti-asymmetrically dimethylated PFKFB3 polyclonal antibody were generated by Sigma-Aldrich Japan (Ishikari, Japan; 5,000× dilution) [10].

2.6. Statistical analysis

All quantitative results are presented as the mean ± SD of independent experiments. Statistical differences between two groups were analyzed by unpaired Student's *t*-test. For experiments with multiple comparisons, data were first analyzed by analysis of

Please cite this article in press as: Mitsuyo Ohmura, et al., Impacts of CD44 knockdown in cancer cells on tumor and host metabolic systems revealed by quantitative imaging mass spectrometry, Nitric Oxide (2014), doi: 10.1016/j.niox.2014.11.005

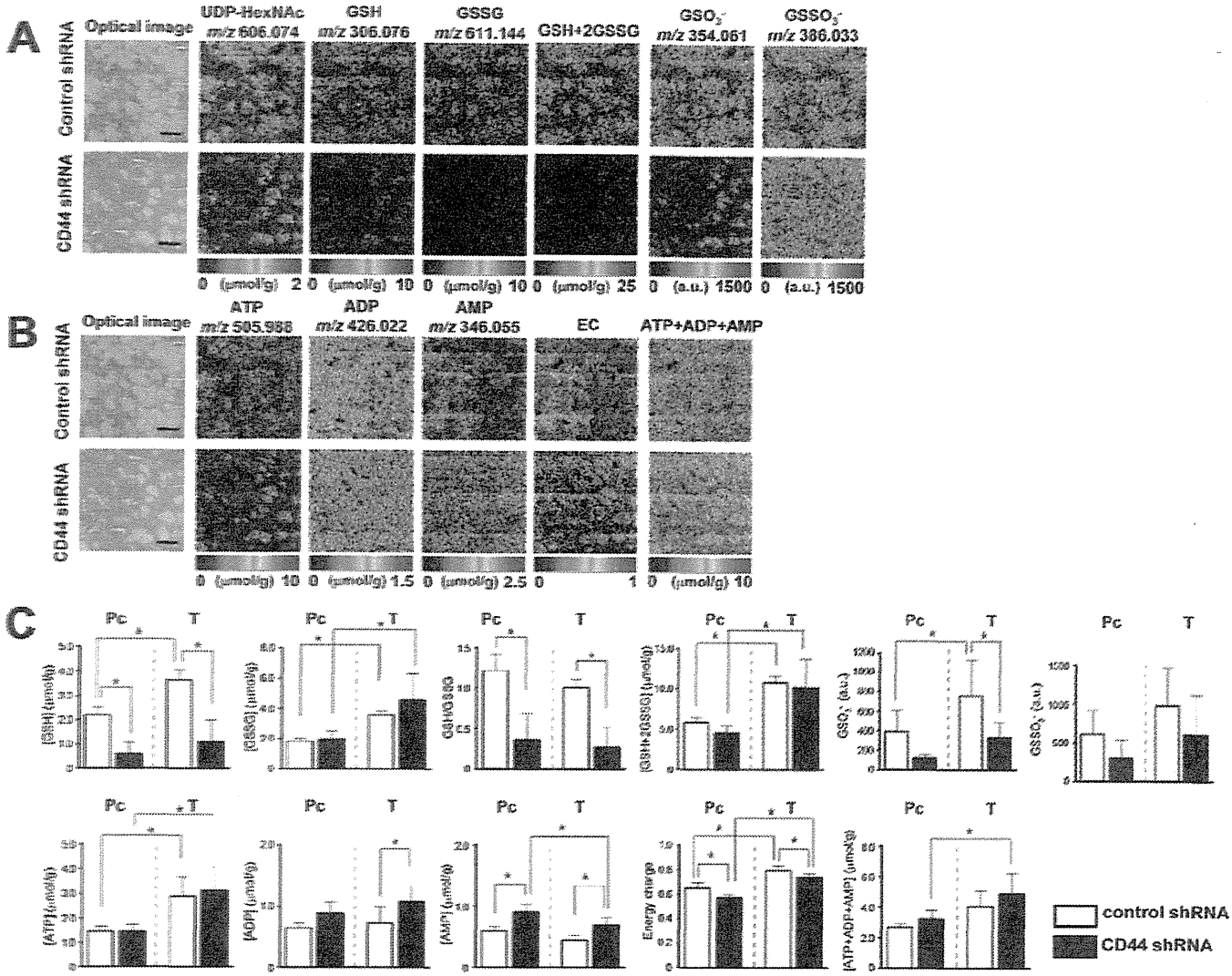

Fig. 3. CD44 knockdown in HCT116 cells decreases GSH and energy charge in tumors and the host liver. A and B. By negative-mode quantitative IMS with scanning mass range of *m/z* 304–670, decreases in GSH, GSH/GSSG and GSO_3^- in both liver parenchyma and tumors and decreases in energy charge (EC) were observed in the liver metastasized by shCD44-treated HCT116 cells. The resolution of this measurement was 10-μm pitch at 250 × 250 spots. Left panels are optical images which were obtained before IMS measurement. Color bar and associated numbers under images indicate apparent amounts of metabolites expressed as μmol/g tissue. Scale bar: 500 μm. Optical images were identical in Panels A and B. C. Quantitative determination of apparent contents metabolites in liver parenchyma (Pc) and tumor regions (T) which control shRNA or CD44 shRNA cells was transplanted for 2 weeks. $^{**}p < 0.01$ and $^{*}p < 0.05$. Values indicate apparent amounts of metabolites expressed as μmol/g tissue. Data indicate mean ± SD of 4–6 mice for each group. ANOVA with Fisher's multiple comparison test was used.

variance (ANOVA) with Fisher's least significant difference. $P < 0.05$ was considered statistically significant.

3. Results

3.1. Characterization of HCT116 cells treated with CD44 knockdown

Fig. 1 indicated characterization of HCT116 cells knocking down CD44 by shRNA treatment. As judged by FACS analysis, short hairpin RNA interference for CD44 (shCD44) down-regulated expression of CD44 in HCT116 cells (Fig. 1A). Western blot analyses showed down-regulation of CD44 proteins that coincided with significant suppression of CBS protein but not that of CSE and methylated PFKFB3 and total PFKFB3, which are determinants of glucose oxidation and energy metabolism (Figs. 1B and 1C) [10]. Under these circumstances, the cancer cells treated with shCD44 exhibited comparable levels of cell proliferation to those treated with control shRNA during 4 days after inoculation of the cells.

3.2. Positive-mode Q-IMS of the liver bearing HCT116-derived tumors

HCT116 cells treated with control shRNA or those with shCD44 were injected into spleens of NOG mice, and liver tissues were examined by Q-IMS (Fig. 2). As seen in Fig. 2A, shCD44 treatment significantly diminished cross-sectional areas of metastatic tumors in the liver tissues. Figs. 2B and 2C depicted representative pictures of metabolites and their quantitative contents in parenchyma (Pc) and tumors (T); all metabolites were measured by positive ion mode using DHB as a matrix reagent. As seen, SAM (*m/z* 399.145) and SAH (*m/z* 385.129) were detectable in a manner comparable between Pc and T. Contents of these metabolites were not greatly

Please cite this article in press as: Mitsuyo Ohmura, et al., Impacts of CD44 knockdown in cancer cells on tumor and host metabolic systems revealed by quantitative imaging mass spectrometry, Nitric Oxide (2014), doi: 10.1016/j.niox.2014.11.005

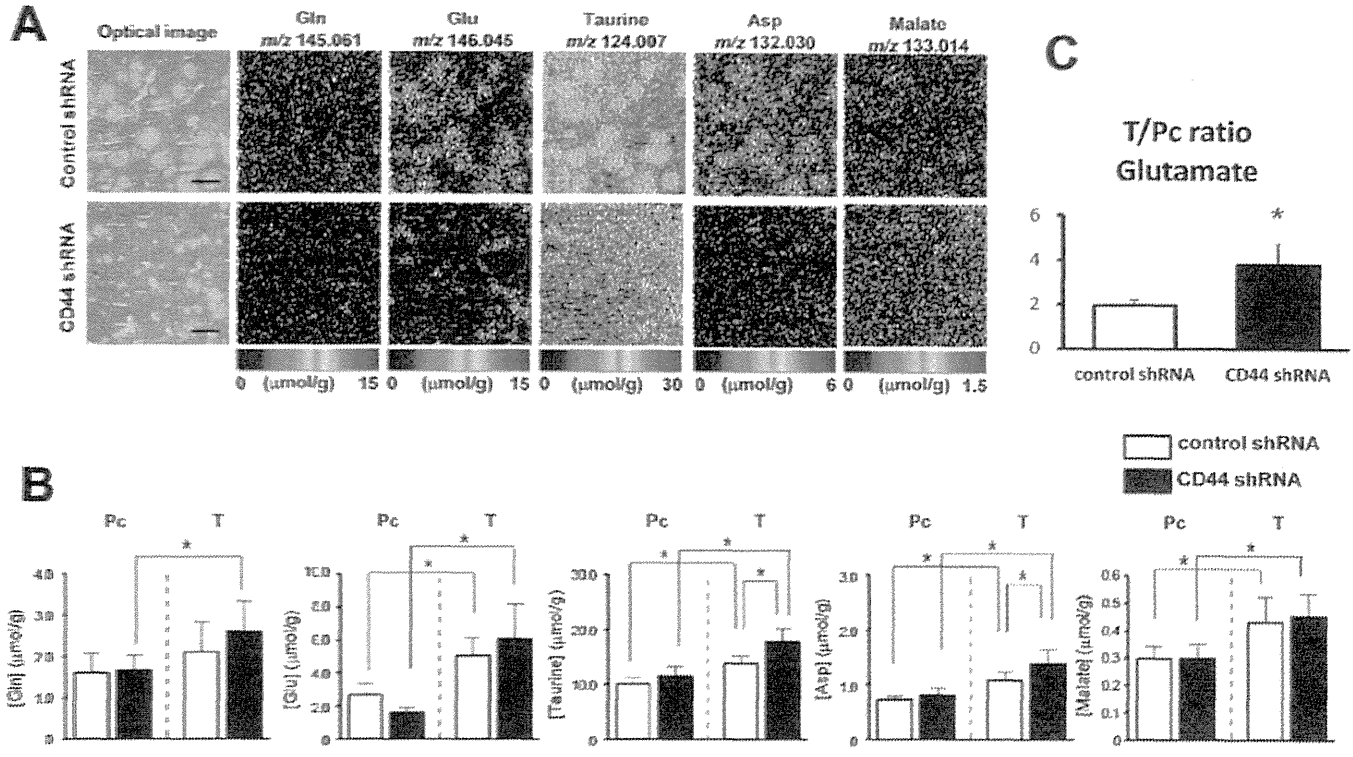

Fig. 4. CD44 knockdown in cancer cells inhibits delivery of glutamate to the host liver. A. By negative-mode quantitative IMS with scanning mass range of *m/z* 86–400, imbalance of glutamate between tumors and the liver and elevation of taurine and aspartate in tumor region were observed. The resolution of this measurement was 25-μm pitch of 100 × 100 spots. Left panels are optical images which were obtained before IMS measurement. Color bar and associated numbers under images indicate apparent amounts of metabolites expressed as μmol/g tissue. Scale bar: 500 μm. B. Quantitative determination of apparent contents metabolites in liver parenchyma (Pc) and tumor regions (T) which control shRNA or CD44 shRNA cells was transplanted for 2 weeks. $^{**}p < 0.01$ and $^{*}p < 0.05$. Values indicate apparent amounts of metabolites expressed as μmol/g tissue. Data indicate mean ± SD of 4–6 mice for each group. ANOVA with Fisher's multiple comparison test was used. C. Ratio of intensity of glutamate signals between tumor regions and liver parenchyma. The data suggest an increase in glutamate in tumor regions. $^{*}p < 0.05$ versus control shRNA. Data indicate mean ± SD of 4–6 mice for each group. Unpaired Student's *t*-test was used.

changed by shCD44 treatment. On the other hand, contents of spermidine and spermine were significantly greater in tumors than in parenchyma. Of note was that shCD44 treatment significantly suppressed contents of spermidine (*m/z* 146.166) and spermine (*m/z* 203.224) in both tumors and parenchyma. Another important change induced by shCD44 was a significant increase in adenosine (*m/z* 268.105) in tumors, which led us to examine energy metabolism using a negative mode MALDI imaging.

3.3. *Negative-mode Q-IMS revealed decreased energy charges and GSH in tumors and the host liver*

Fig. 3 illustrates negative-mode Q-IMS collected by using 9-aminoacridine as a matrix reagent. As previously described, UDP-N-acetyl hexosamine (UDP-HexNAc, *m/z* 606.074) was accumulated in tumors that did not alter in response to shCD44 treatment. In fasted mice treated with control shRNA, contents of GSH (*m/z* 306.076) were greater in tumors than in parenchyma. Treatment with shCD44 significantly suppressed GSH contents in tumors as well as in parenchyma. Contents of GSSG (*m/z* 611.144) were greater in tumors than in parenchyma. In response to shCD44, GSSG showed a modest elevation but without statistical significance. Under these circumstances, Total amounts of glutathione (GSH+2GSSG) were significantly higher in tumors than in parenchyma. Of importance was that no suppression of total glutathione was seen in response to shCD44, suggesting that the amounts appear to be compensated by mechanisms independent of CD44/xCT system (Figs. 3A and 3C).

We have recently shown that a portion of glutathione is oxidized under atmospheric MALDI conditions to form glutathione sulfonate (GSO_3^-, *m/z* 354.061) and serves as a substrate for generating glutathione S-sulfonate ($GSSO_3^-$, *m/z* 386.033) in the presence of endogenous HS^-. In other words, $GSSO_3^-$ serves as an indicator of endogenous HS^- generation [10]. These metabolites in tumors were suppressed by shCD44, while the decrease in $GSSO_3^-$ was marginally significant (Figs. 3A and 3C).

Fig. 3B illustrates alterations in energy metabolism in response to shCD44 treatment. In fasted mice, ATP contents were significantly greater in tumors than in parenchyma. Based on data of ADP and AMP, energy charge (EC) was calculated as ratio images; as seen, EC was higher in tumors than in parenchyma. Furthermore, shCD44 treatment in tumors significantly suppressed EC values not only in tumors but also in parenchyma, suggesting that CD44 in cancer cells mediates mutual interplay for maintaining energy metabolism *in vivo*.

3.4. *Negative-mode Q-IMS reveals that CD44 causes glutamate imbalance between tumors and the liver*

Tumors turned out to accumulate significantly greater amounts of glutamate than parenchyma (Figs. 4A and 4B). In response to shCD44, contents of glutamate (*m/z* 146.045) in parenchyma appeared to decrease with marginally significant levels, while those in tumors conversely displayed a modest elevation. We then calculated T/Pc ratio of glutamate to examine differences between control shRNA and shCD44 groups, showing a significant

Please cite this article in press as: Mitsuyo Ohmura, et al., Impacts of CD44 knockdown in cancer cells on tumor and host metabolic systems revealed by quantitative imaging mass spectrometry, Nitric Oxide (2014), doi: 10.1016/j.niox.2014.11.005

elevation of the ratio in response to shCD44 treatment (Fig. 4C). Considering that CD44/xCT requires glutamate excretion to uptake cystine into cells, these results suggest that CD44 knockdown in cancer cells helps accumulate glutamate in tumors and decrease the delivery of cystine from parenchyma.

Another important observation was the fact that shCD44 treatment increases contents of taurine (*m/z* 124.007) and aspartate (*m/z* 132.030) in tumors but not in parenchyma; the interpretation of these findings will be discussed later.

3.5. *Metabolome analyses of HCT116 cells in culture*

Fig. 5 illustrates differences in metabolomic profiling between HCT116 cells treated with control shRNA and those with shCD44 in culture. In these experiments, the cells were cultured for 72 hrs at which no difference in cell growth was observed (Fig. 1D). CE-MS analyses revealed that shCD44 treatment decreased significantly total amounts of metabolites belonging to methionine salvage pathway (MS; spermidine and spermine) and remethylation (RM) and transsulfuration (TS) pathways; amounts of metabolites residing above cysteine in Fig. 5 (Σ(MS + RM + TS)) in shCD44-treated cells were significantly smaller than those treated with control shRNA. Of note is the observation that, despite decreased expression of CBS in response to CD44 knockdown, cystathionine is not decreased. Such observation appeared consistent with a notion that CD44 knockdown may increase supply and delivery of the MS and RM substrates to the downstream pathway.

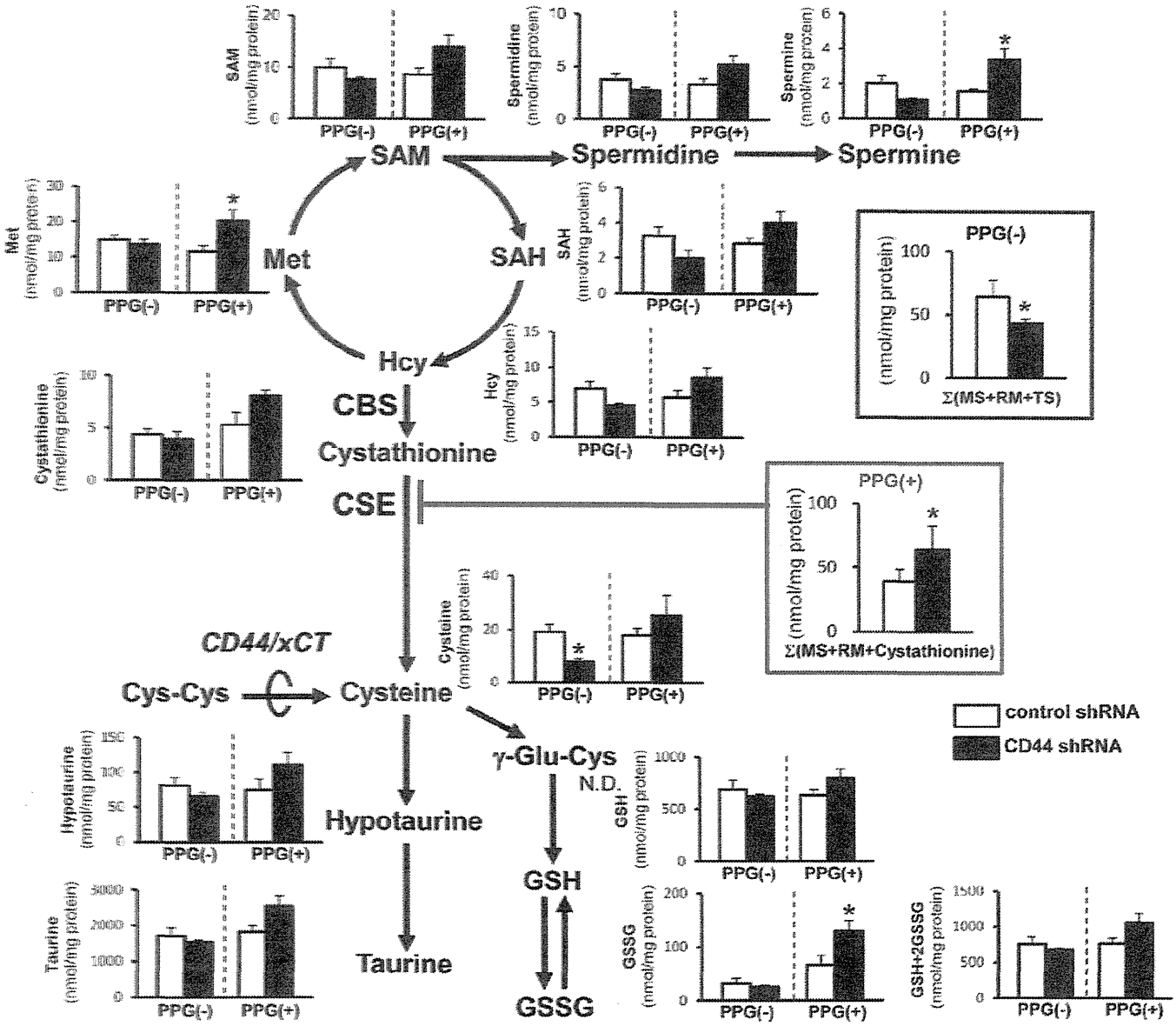

Fig. 5. Alterations in metabolites in methionine salvage, remethylation and transsulfuration pathways in shCD44-treated HCT116 cells in culture. HCT116 cells treated with control shRNA (open bars) and CD44 shRNA (filled bars) were incubated for 72 hours with the medium of DMEM containing 3.15 g/L glucose. The metabolites were measured by capillary electrophoresis with mass spectrometry (CE-MS). Σ(MS + RM + TS: methionine salvage pathway (MS) + remethylation (RM) + transsulfuration (TS)) is expressed as total sum values of Met, SAM, SAH, spermidine, spermine, Hcy, cystathionine, and Cys. $^{*}p < 0.05$ versus control shRNA cells. Data indicate mean ± SD of 4–5 separate experiments. Unpaired Student's *t*-test was used.

Please cite this article in press as: Mitsuyo Ohmura, et al., Impacts of CD44 knockdown in cancer cells on tumor and host metabolic systems revealed by quantitative imaging mass spectrometry, Nitric Oxide (2014), doi: 10.1016/j.niox.2014.11.005

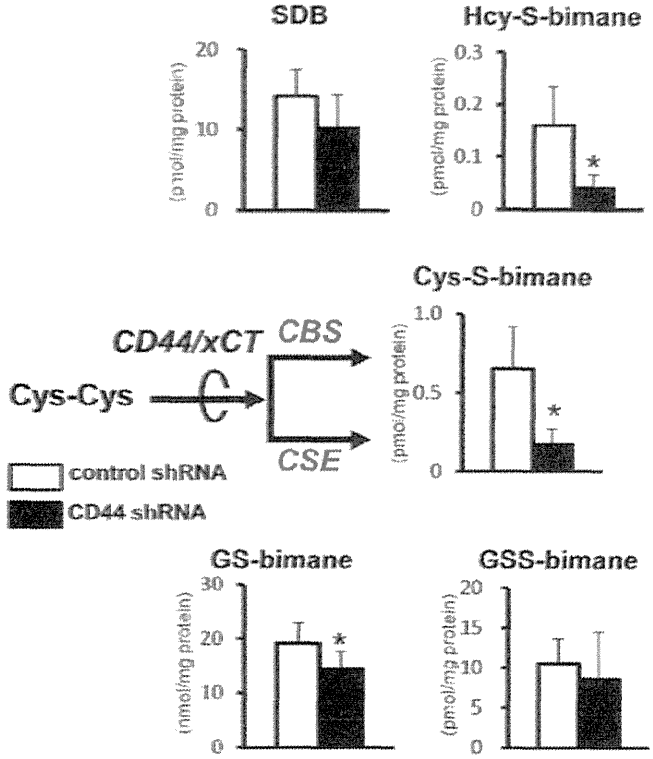

Fig. 6. Effects of shCD44 on reactive cysteine persulfide and related persulfide compounds detected by monobromobimane derivatization methods. $^{*}p < 0.05$ versus control shRNA cells. Data indicate mean ± SD of 6 separate experiments. Unpaired Student's *t*-test was used.

We also examined effects of CSE inhibition by propargylglycine (PPG) in the control and shCD44-treated HCT116 cells in culture (right panels of individual graphs of Fig. 5). Interestingly, PPG treatment significantly increased methionine and spermine and caused marginally significant increases in SAM, SAH, spermidine and homocysteine (Hcy); as a result, the PPG treatment caused a significant elevation of Σ(MS + RM + cystathionine) values in shCD44-treated cells but not in the control cells. PPG treatment also exhibited a significant elevation of GSSG but not that of GSH. Collectively, combined treatment with CD44 knockdown and PPG appeared to increase metabolites of remethylation cycle and decreased the antioxidative capacity of the cancer cells.

Since CE-MS protocols include treatment with acid that disturbs accurate GSH measurements, we attempted to stop redox conversion of the compound by derivatization using MBB. This technique also benefits measurements of reactive thiol compounds including cysteine persulfide and glutathione persulfide in the cells. As seen in Fig. 6, amounts of cysteine persulfide and homocysteine persulfide that are thought to be generated through CBS and CSE from cystine (Cys-Cys) and homocystine (Hcy-Hcy), respectively, were significantly reduced by shCD44 treatment. On the other hand, glutathione persulfide adduct (GSS-bimane) was not significantly suppressed by shCD44 treatment. However, amounts of GS-bimane adduct were significantly suppressed. Considering that cysteine persulfide is a primary product of varied reactive persulfides generated by CBS and CSE using cystine as a substrate [5], these results suggested that CD44 expression is necessary to maintain contents of reactive cysteine persulfides and GSH in cancer cells.

These results collected from experiments *in vitro* as well as those *in vivo* led us to hypothesize that cancer cells consume metabolites belonging to MS, RM and TS pathways as an adaptive response against CD44 knockdown. In order to test this hypothesis, effects of either PPG for blocking CSE or cessation of methionine or cystine in culture were examined in the same cell culture system (Fig. 7). The control shRNA-treated cells were able to maintain the cell number in the presence of PPG, while shCD44-treated cells exhibited a significant reduction of the cell number, indicating greater dependence on transsulfuration pathway for survival (Fig. 7A). In the absence of methionine in the culture medium, both cell types exhibited significant decreases in the cell number, showing ~80% drop versus the methionine-containing controls. In the absence of methionine, shCD44-treated cells displayed greater sensitivity than the cells treated with control shRNA (Fig. 7B). These results suggest

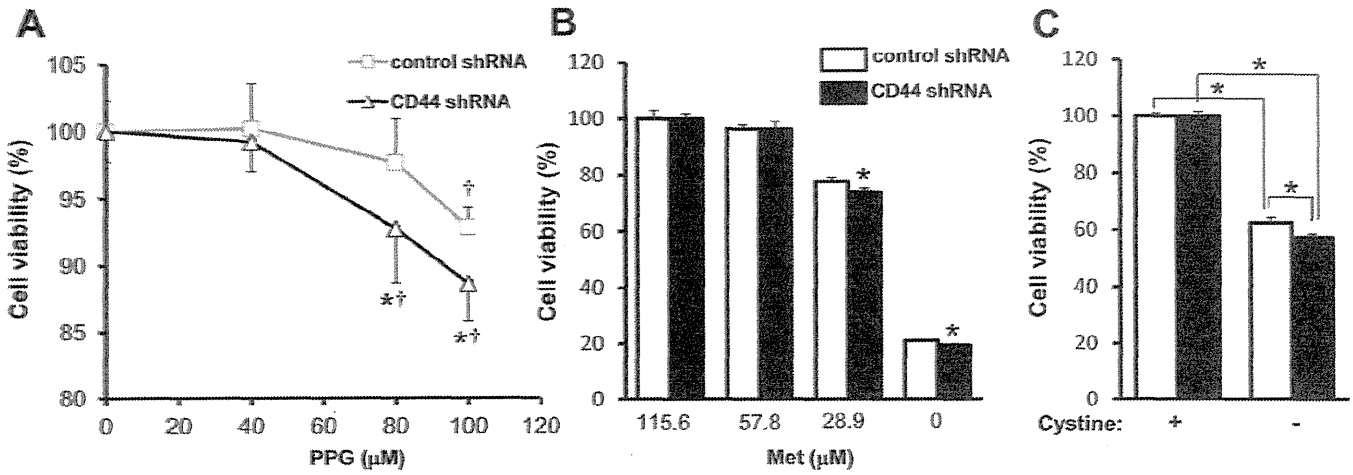

Fig. 7. Different sensitivity between shCD44 and control shRNA-treated HCT116 cells to CSE inhibitor propargylglycine (PPG) and methionine cessation in culture. A. Effects of CD44 knockdown on 115.6 μM methionine (Met) with varied concentrations of propagylglycine (PPG). Cell viability was measured by Cell Counting Kit 8. Data indicate mean ± SD of 5 wells for each group. $^{*}p < 0.05$ versus the control shRNA-treated groups with the same concentrations of PPG. †$p < 0.05$ versus the PPG-free groups. ANOVA with Fisher's multiple comparison test was used. B. Greater sensitivity of shCD44-treated HCT116 cells to methionine cessation. Cell viability on 4 different methionine concentrations was examined by Cell Counting Kit 8. Data indicate mean ± SD of 6 separate experiments for each groups. $^{*}p < 0.05$ versus control shRNA cells. Unpaired Student's *t*-test was used. C. Effects of cessation of cystine on the cell viability of HCT116 cells treated with control shRNA and those with shCD44. $^{*}p < 0.05$ versus control shRNA cells. ANOVA with Fisher's multiple comparison test was used.

Please cite this article in press as: Mitsuyo Ohmura, et al., Impacts of CD44 knockdown in cancer cells on tumor and host metabolic systems revealed by quantitative imaging mass spectrometry, Nitric Oxide (2014), doi: 10.1016/j.niox.2014.11.005

that shCD44-treated cancer cells depend on methionine and its related metabolites to greater extents than the control cells. We also tested effects of cessation of cystine on the cell viability (Fig. 7C). As seen, cessation of cystine significantly decreased the cell viability approximately by 40%, while shCD44-treated cells exhibited greater sensitivity than those treated with the control shRNA.

It was technically difficult to examine the effects of methionine cessation on metabolome because the majority of the cells lost their viability. Since the cystine cessation caused a modest cell injury, we attempted to compare the methionine-related metabolome between the cells in the presence or absence of cystine (Fig. 8). As seen, cessation of cystine caused a significant elevation of Σ(MS + RM + TS) values in both control shRNA- and shCD44-treated HCT116 cells. These results suggest that metabolites belonging to methionine salvage and remethylation pathways are compensated in response to cystine cessation through CD44-independent mechanisms.

4. Discussion

4.1. CD44 in cancer cells regulates tumor-host metabolic interactions in vivo

We showed that targeting CD44 in cancer cells does not only affect their metabolic systems but also alters metabolic responses of the liver as a host tissue. Up to now, CD44 has been shown to interact with xCT in many cancer cell lines, and its down-regulation lowers the stability of xCT that decreases incorporation of cystine and cysteine, compromising the capacity of glutathione to ameliorate oxidative stress [17,18]. On the other hand, CD44 interacts with PKM2 to maintain Warburg effect; the CD44 RNA interference causes interaction with PKM2 and accelerates glucose oxidation in mitochondria that secondarily results in oxidative stress and jeopardizes the viability of cancer cells [18]. In this study, shCD44 significantly suppresses tumor growth. Even under these circumstances,

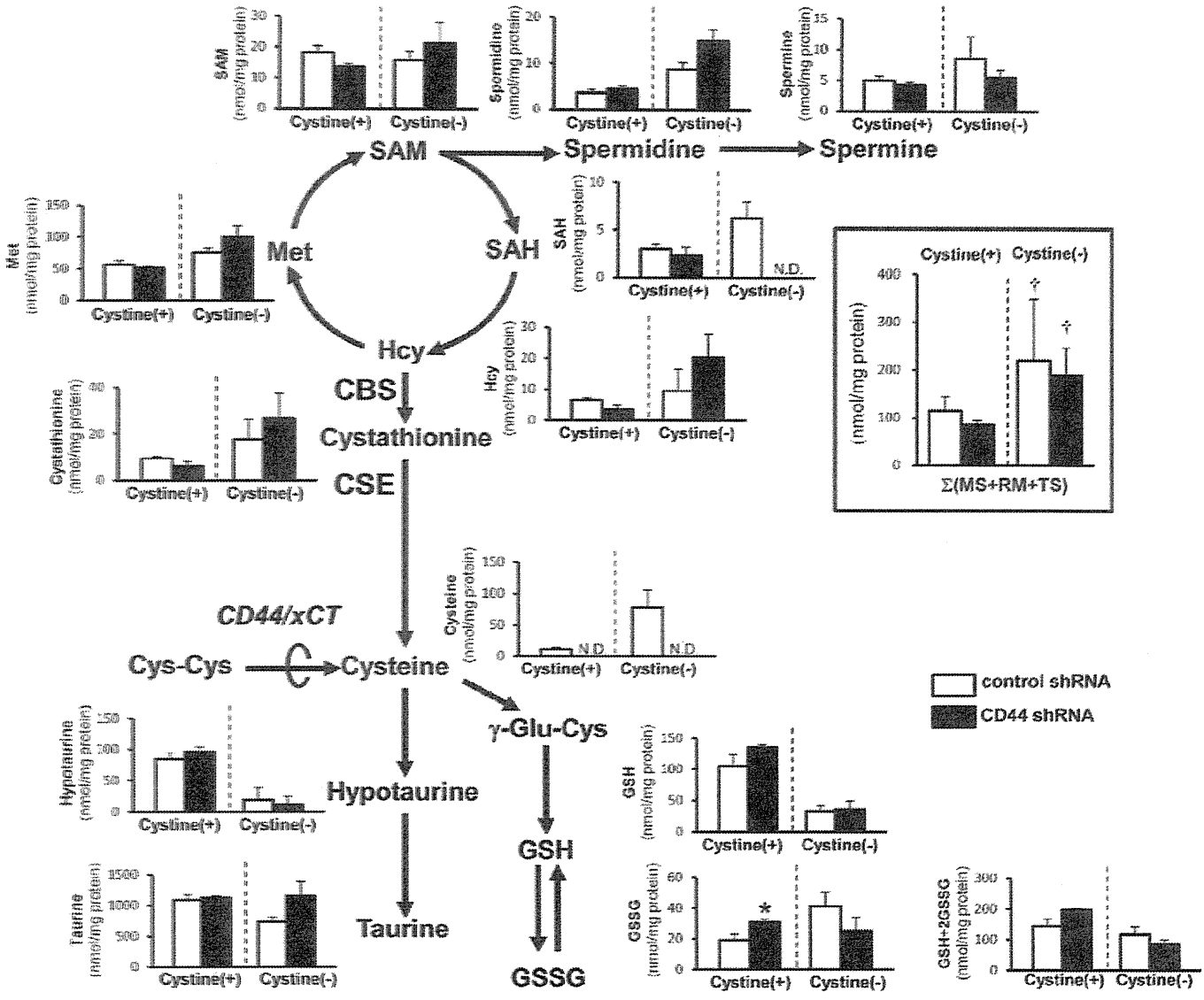

Fig. 8. Differences in contents of methionine-related metabolites between HCT116 cells treated with or without cystine in culture. *$p < 0.05$ versus the control shRNA. Unpaired Student's *t*-test was used. †$p < 0.05$ versus the data of the cells cultured in cystine-containing medium. For the intergroup comparison, ANOVA with Fisher's multiple comparison test was used.

Please cite this article in press as: Mitsuyo Ohmura, et al., Impacts of CD44 knockdown in cancer cells on tumor and host metabolic systems revealed by quantitative imaging mass spectrometry, Nitric Oxide (2014), doi: 10.1016/j.niox.2014.11.005